optica

Microwave-optical quantum frequency conversion

Xu Han,[1,2] Wei Fu,[1] Chang-Ling Zou,[3] Liang Jiang,[4] and Hong X. Tang[1,5,*]

[1]Department of Electrical Engineering, Yale University, New Haven, Connecticut 06520, USA
[2]Center for Nanoscale Materials, Argonne National Laboratory, Argonne, Illinois 60439, USA
[3]Department of Optics and Optical Engineering, University of Science and Technology of China, Hefei, Anhui 230026, China
[4]Pritzker School of Molecular Engineering, The University of Chicago, Chicago, Illinois 60637, USA
[5]Yale Quantum Institute, Yale University, New Haven, Connecticut 06520, USA
*Corresponding author: hong.tang@yale.edu

Received 17 March 2021; revised 6 June 2021; accepted 23 June 2021 (Doc. ID 425414); published 2 August 2021

Photons at microwave and optical frequencies are principal carriers for quantum information. While microwave photons can be effectively controlled at the local circuit level, optical photons can propagate over long distances. High-fidelity conversion between microwave and optical photons will allow the distribution of quantum states across different quantum technology nodes and enhance the scalability of hybrid quantum systems toward a future "Quantum Internet." Despite a frequency difference of five orders of magnitude, there has been significant progress recently toward the transfer between microwave and optical photons with steadily improved efficiency in a coherent and bidirectional manner. In this review, we summarize this progress, emphasizing integrated device approaches, and provide a perspective for device implementation that enables quantum state transfer and entanglement distribution across microwave and optical domains.

https://doi.org/10.1364/OPTICA.425414

1. INTRODUCTION

Electromagnetic waves at microwave and optical frequencies are the most widely deployed signal carriers in today's information processing and communication systems. They also play pivotal roles in encoding quantum information. Over the past decades, a variety of qubit systems have been developed, some exploiting excitations at optical frequencies, including trapped ions [1], neutral atoms [2], quantum dots [3,4], and solid-state defects [5,6], and others operating at microwave frequencies including superconducting qubits [7] and spins in crystals [8]. Among these, superconducting qubits stand out as one of the most promising quantum computing platforms. In superconducting quantum circuits, the low-loss single-photon nonlinearity at microwave frequencies inherent to the Josephson effect allows high-fidelity quantum operations approaching error-correction thresholds [7,9–11]. Based on this circuit quantum electrodynamics (cQED) architecture, a prototype quantum computer having more than 50 qubits has been developed [12,13].

However, quantum states encoded in microwave photons are localized at millikelvin stages of a dilution refrigerator and would be swamped by thermal noise when emerging to room temperature. The high transmission loss of a microwave signal at room temperature further prevents the propagation of quantum signals over a long distance. Optical photons, on the other hand, show complementary features and are the ideal information carrier for communications over large spatial scales, for example, more than 100 km in fibers [14] and beyond 1000 km in free space [15]. Therefore, the ability to transfer quantum states encoded at microwave frequencies to optical light would greatly enrich cQED as a platform for quantum information processing and expand the quantum computing network, as well as establish new forms of quantum communication links.

Through a high-fidelity microwave–optical (M-O) converter, microwave quantum circuits could also access long lived quantum memory via optical interfaces. Despite the rapid advances [16], the 100 μs to ms lifetimes afforded by superconducting qubits are still relatively short compared with the 100 s lifetime obtained using ions [17], and the several hours lifetime in nitrogen-vacancy (NV) centers [18] and rare-earth spin ensembles [19]. Clearly, a hybrid quantum system with the complementary traits of superconducting qubits and optically addressable quantum memories would offer a tremendous advance in quantum information science [20,21].

Conversely, room-temperature quantum optic circuits, by way of M-O conversion, could benefit from on-demand microwave photon sources and high-fidelity microwave photon detectors provided by the state-of-the-art cQED systems. As of today, an on-demand single photon source remains a major challenge in the quantum photonics community. In microwave circuits, with the help of superconducting qubits, on-demand single microwave photons can be reliably generated [22,23]. It can be envisioned that such microwave photons can be upconverted to on-demand single optical photons with an ideal, lossless M-O converter. Similarly, superconducting qubits and arrays could perform as photon number resolved detectors, which represent another bottleneck in quantum photonics, to analyze downconverted quantum optical states.

Hence a future distributed quantum network could exploit the quantum information processing ability at the microwave frequency and low quantum decoherence at the optical frequency simultaneously. The ideal method to combine microwave and optical technologies is an integrated device platform that incorporates superconducting and nanophotonic devices on a single chip, and allows coherent photon transduction between microwave and optical frequencies without incurring interconnection losses.

What microwaves in superconducting circuits and light waves in optical networks have in common is their ultralow loss, which leads to their exploitation in ultrafast digital signal processing and high-rate data transmission, respectively, in superconductors and optical fibers. When combined on a single chip platform, they offers further advantages to improve device performances in classical applications. For example, optical technology can retrieve massive data generated at cryogenic digital data processors, by either superconducting single-flux-quantum (SFQ) logic circuits [24] or cryogenic CMOS processors [25]. On the other hand, superconducting nanowires and high-kinetic inductance devices have become efficient detectors of optical signals [26].

M-O converters must involve nonlinear processes to compensate for the large energy difference between microwave and optical photons; direct M-O coupling is extremely weak. Many schemes have been investigated to boost the coupling with a wide range of nonlinear frequency mixing mechanisms, including optomechanics, electro-optics, optomagnonics, solid-state spins, trapped atoms/ions, etc. Our goal is to provide a review of current approaches of M-O systems, the underlying nonlinear processes, and the desired metrics for M-O conversion with emphasis on integrated chip-scale device implementations.

2. OUTLINE OF THIS REVIEW

This is a topical review on M-O quantum frequency conversion with a particular focus on photonic chip-based approaches. We also refer advanced readers to several recent review articles related to this topic [21,27–31]. We will set the stage by introducing the nonlinear and parametric processes involved in the M-O photon conversion, and outline the figures of merit (Section 3). Then we will briefly discuss what have been accomplished in intraband frequency conversions (Section 4), particularly on the microwave-to-microwave conversion aided by superconductivity and the optical-to-optical conversion aided by the nonlinear Kerr effect in photonics. The interband conversions including microwave-to-optics conversion can be regarded as extensions of intraband conversion processes and share similar nonlinear optics principles. In the sections that follow, we move on to discuss and compare various schemes for M-O conversion that are being attempted on different platforms. In particular, we will highlight three distinct conversion schemes: electro-optomechanics (Section 5), electro-optics (Section 6), and optomagnonics (Section 7), followed by a brief discussion on atom-assisted conversion (Section 8). Finally, we give an outlook of cross-platform quantum transduction and lay out the challenges and opportunities in this exciting field (Section 9).

3. NONLINEAR PROCESSES IN MICROWAVE-TO-OPTICAL FREQUENCY CONVERSION

Nonlinearity plays a crucial role in M-O frequency conversion, because it allows the use of an external pump to compensate for the energy difference between the microwave and optical modes, while maintaining the phase coherence between input and output signals. In this section, we first classify various types of nonlinear processes and use this classification to describe various M-O photon conversion schemes. Then we linearize the coupled system under the condition of strong external pumps, so that we can employ input–output theory to compute the key characteristics such as conversion efficiency, bandwidth, and added noise.

A. Nonlinear Interactions

We may classify nonlinear processes by the order of nonlinearity of their interaction Hamiltonian. We expand the Hamiltonian coupling different bosonic modes (with operator m_j for the jth mode and $c_{j\ldots}$ for constant coefficients) in the following form:

$$H = H_1 + H_2 + H_3 + H_4 + \cdots, \tag{1}$$

where $H_1 = \hbar \sum_j (c_j m_j^\dagger + \text{h.c.})$ is the external drive, $H_2 = \hbar \sum_{j,k} (c_{j,k} m_j^\dagger m_k + c'_{j,k} m_j^\dagger m_k^\dagger + \text{h.c.})$ is the $\chi^{(1)}$ process that is quadratic in mode creation and annihilation operators, $H_3 = \hbar \sum_{j,k,l} (c_{j,k,l} m_j^\dagger m_k^\dagger m_l^\dagger + c'_{j,k,l} m_j^\dagger m_k^\dagger m_l + \text{h.c.})$ is the $\chi^{(2)}$ process, and so on. The linear process refers to the dynamics associated with H_1 and H_2 only, because the Heisenberg equation of motion $\frac{dO}{dt} = \frac{i}{\hbar}[H, O]$ is a closed set of linear equations for the mode operators O (i.e., creation and annihilation operators of the relevant modes). All the higher order terms (H_3, H_4, …) are nonlinear processes, because their commutators with mode operators generate quadratic or higher order terms. Following the convention from nonlinear optics, the nonlinear process associated with Hamiltonian H_{n+1} is called a $\chi^{(n)}$ process, because the commutator $[H_{n+1}, O]$ between the Hamiltonian and mode operator has order n in the Heisenberg equation. While the linear processes of H_1 and H_2 induce only constant and linear terms in the Heisenberg equation, which can be easily solved by linear differential equations, the higher order Hamiltonian terms (e.g., $H_{n\geq 3}$ for $\chi^{(n\geq 2)}$ processes) give nonlinear terms in the Heisenberg equation, which lead to interesting nonlinear dynamics including coherent photon conversions.

As shown in Fig. 1(a), we may use simple diagrams to illustrate different $\chi^{(n)}$ processes. For example, the piezoelectric effect has a quadratic Hamiltonian H_2 associated with the $\chi^{(1)}$ linear process. The electro-optic effect, optomechanical coupling due to radiation pressure, and electrostriction effect can all be described by a cubic Hamiltonian H_3 associated with a $\chi^{(2)}$ nonlinear process. The four-wave mixing process has a quartic Hamiltonian H_4 associated with a $\chi^{(3)}$ nonlinear process. Moreover, we can combine lower order processes to generate new nonlinear couplings. As illustrated in Fig. 1(b), we can combine a $\chi^{(1)}$ process and a $\chi^{(2)}$ process to generate a new *effective* $\chi^{(2)}$ process, which can describe the combined piezoelectric and optomechanical effects for M-O photon conversion. When we combine two $\chi^{(2)}$ processes, we can generate an *effective* $\chi^{(3)}$ process, which can describe the electro-optomechanical and the electro-optomagnonic conversion schemes.

(a)

	$\chi^{(1)}$ process	$\chi^{(2)}$ process	$\chi^{(3)}$ process
Hamiltonian	$(m_1 + m_1^\dagger)(m_2 + m_2^\dagger)$	$m_1^\dagger m_1 (m_2 + m_2^\dagger)$	$m_1^\dagger m_2^\dagger m_3 m_4 + m_1 m_2 m_3^\dagger m_4^\dagger$
Processes	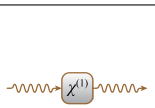	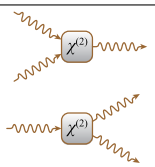	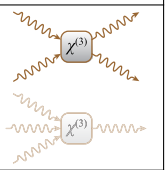
Examples	Piezoelectric Effect	Electro-optic Effect Electromechanical Effect Optomechanical Effect	Four-wave Mixing

(b) **Rules for Combining Processes:**

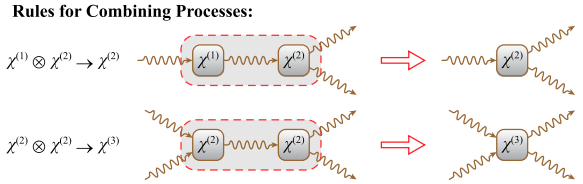

Fig. 1. (a) Classification and diagrams of $\chi^{(1)}$, $\chi^{(2)}$, and $\chi^{(3)}$ processes. (b) Rules for combining processes to generate new and higher order processes.

(a)

	$\chi^{(1)}$ process	$\chi^{(2)}$ process
Electro-optic (EO)	Energy Mismatch	Electro-optic Modulator $H_{eo} = \hbar g_{eo,0} a^\dagger a (b + b^\dagger)$
Electromechanical (EM)	Piezoelectric Effect $H_{pz} = \hbar g_{pz} (b + b^\dagger)(m + m^\dagger)$	Moving Capacitor $H_{em} = \hbar g_{em,0} b^\dagger b (m + m^\dagger)$
Optomechanical (OM)	Energy Mismatch	Radiation Pressure $H_{om} = \hbar g_{om,0} a^\dagger a (m + m^\dagger)$
Magneto-optical (MO)	Energy Mismatch	Faraday Effect $H_{mago} = \hbar g_{mago,0} a^\dagger a (m + m^\dagger)$

(b)

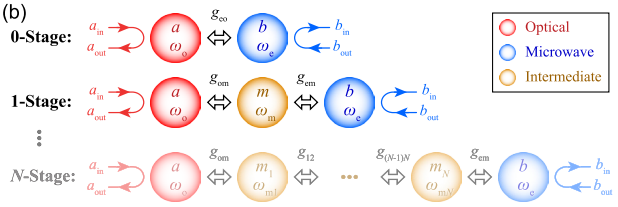

Fig. 2. (a) Hamiltonians for various couplings relevant to microwave-to-optical mode conversions. (b) Illustration of the conversion pathway between optical (a) and microwave (b) modes. In general, the conversion process can involve N intermediate modes (m_j with $j = 1, \ldots, N$), with $N = 0$ representing the direct electro-optic conversion.

In Fig. 2(a), we list various coupling mechanisms relevant to M-O photon conversion with their Hamiltonians. To harness the nonlinear processes for coherent linear conversion, a red-detuned optical pump tone is required to compensate for the energy difference between the target coupled modes. For example, for electro-optic coupling $H_{eo} = \hbar g_{eo,0} a^\dagger a (b + b^\dagger)$, application of a red-detuned optical pump will reduce the Hamiltonian to the "beam splitter" form $H_{eo} \approx \hbar g_{eo} (a^\dagger b + b^\dagger a)$ in the resolved-sideband limit ($\omega_e \gg \kappa_o$). Here, $g_{eo,0}$ is the single-photon electro-optic coupling rate, and a (b) and ω_o (ω_e) denote the annihilation operator and resonant frequency of the optical (microwave) mode, respectively. $g_{eo} = g_{eo,0}\sqrt{n_{cav,o}}$ is the cavity-enhanced coupling rate, with $n_{cav,o}$ being the pump photon number in the optical cavity. Therefore, the external pump(s) can not only compensate for the energy difference between the input and output modes, but also enhance the coupling via the bosonic enhancement factor(s) of $\sqrt{n_{cav,o}}$. A similar linearization process can be obtained for other types of $\chi^{(2)}$ coupling. This review mainly focuses on the above-discussed SWAP-based transduction that relies on the beam splitter interaction. Quantum transduction based on other types of two-mode interaction also exists [32–35], and will be discussed briefly in the Section 9.

B. Conversion Efficiency and Added Noise

In general, the M-O conversion can be achieved through N intermediate modes [as shown in Fig. 2(b)], where the coupling between adjacent modes is characterized by a linearized coupling rate g_{ij}. We use standard input–output formalism to characterize the dynamics of the intermediate and output modes as a function of the input modes [36]. Denoting intra-cavity fields of all the modes as $\mathbf{a}(t) = (a, m_1, \ldots, m_N, b)^T$, the Heisenberg equation of motion of the N-stage conversion system can then be expressed as

$$\dot{\mathbf{a}}(t) = \mathbf{A}\mathbf{a}(t) + \mathbf{B}\mathbf{a}_{\mathbf{in}}(t), \tag{2}$$

where $\mathbf{a_{in}}(t) = (a_{\text{in,ext}}, a_{\text{in,int}}, m_{1\text{in,int}}, \ldots, m_{N\text{in,int}}, b_{\text{in,ext}}, b_{\text{in,int}})^T$ is the input field. The "ext" and "int" in the second subscript index denote the external coupling and the intrinsic loss (noise) of the ports, respectively, and we have assumed that each intermediate mode has only an intrinsic port. Note that we have assumed a "one-port" coupling configuration for both the microwave and the optical modes, which is necessary for achieving the ideal 100% conversion efficiency. Matrices $\mathbf{A}$ and $\mathbf{B}$ are given in Appendix A.

Combined with the input–output relation

$$\mathbf{a_{out}}(t) = \mathbf{B}^T\mathbf{a}(t) - \mathbf{a_{in}}(t), \tag{3}$$

one can solve Eq. (2) in frequency domain and obtain the scattering matrix $\mathbf{S}[\omega]$ (defined by $\mathbf{a_{out}}[\omega] = \mathbf{S}[\omega]\mathbf{a_{in}}[\omega]$) as

$$\mathbf{S}[\omega] = \mathbf{B}^T[-i\omega\mathbf{I}_{N+2} - \mathbf{A}]^{-1}\mathbf{B} - \mathbf{I}_{N+4}, \tag{4}$$

where $\mathbf{I}_j$ denotes the $(j \times j)$ identity matrix.

The conversion efficiency, bandwidth, and added noise can be fully obtained from the scattering matrix elements. As the general results for N-stage M-O conversion are complex, to better reveal the physics, in the following, we will focus on the simplest cases of zero- (direct) and one-stage conversions, which are also most relevant in experiment. When the parametric pump is red-detuned by the resonant frequency of the microwave mode (or the intermediate mode for one-stage conversion), the photon number conversion efficiency (η) at zero detuning can be simply expressed in terms of the cooperativities (see Appendix A for details).

For zero-stage (direct) conversion,

$$\eta = \eta_o \eta_e \frac{4C_{eo}}{(1 + C_{eo})^2}, \tag{5}$$

and for one-stage conversion,

$$\eta = \eta_o \eta_e \frac{4C_{om}C_{em}}{(1 + C_{om} + C_{em})^2}. \tag{6}$$

Here, $\eta_o = \frac{\kappa_{o,ext}}{\kappa_o}$ and $\eta_e = \frac{\kappa_{e,ext}}{\kappa_e}$ are the extraction factors given by the ratio between the external coupling rates ($\kappa_{o,ext}$ and $\kappa_{e,ext}$) and the total dissipation rates (κ_o and κ_e) of the optical and the microwave modes, respectively. $C_{ij} \equiv \frac{4g_{ij}^2}{\kappa_i \kappa_j}$, where

$(i, j) = (\mathrm{o}, \mathrm{m}, \mathrm{e})$ is the cooperativity between modes i and j. Another useful definition is the so-called "internal efficiency," which characterizes the conversion within the cavities without taking into account the photon extraction ratios at the ports, given by $\eta_{\mathrm{in}} = \eta/(\eta_{\mathrm{e}}\eta_{\mathrm{o}})$.

It can be seen that, to obtain 100% M-O photon conversion efficiency, highly over-coupled ports ($\eta_{\mathrm{o}}, \eta_{\mathrm{e}} \to 1$) are necessary for both cases, and the cooperativities should satisfy the matching conditions ($C_{\mathrm{eo}} = 1$) and ($C_{\mathrm{om}} = C_{\mathrm{em}} \gg 1$) for the direct and one-stage conversions, respectively.

Besides a high conversion efficiency, it is also crucial to maintain low added noise (n_{add}), which is defined as the equivalent noise referring to the input (namely, the noise at the output divided by conversion efficiency). This definition well characterizes the influence of the noise on the input signal in spite of the conversion efficiency. A similar definition of added noise is broadly used for amplifiers [37]. The added noise has two major contributions—environmental thermal noise and undesired parametric processes. In the resolved-sideband regime ($\omega_{\mathrm{e,m}} \gg \kappa_{\mathrm{o,e}}$), the parametric noise is favorably suppressed by a factor of $\sim(\kappa_{\mathrm{o,e}}/\omega_{\mathrm{e,m}})^2$ [38]. For most platforms discussed in this review paper, we are in the deep resolved-sideband regime, so the contribution from parametric processes is relatively small compared to the environmental noise. For other platforms (e.g., when the mechanical mode has a relatively low frequency), it is important to include the parametric processes, which may amplify the output signal while adding extra noise due to amplification.

For the environmental thermal noise, it is a good model to assume that inputs from different environmental noise sources are not correlated in most situations, so that we can simply characterize each environmental noise source by using its average thermal occupation, which is given by $\bar{n}_{\mathrm{th}} = (e^{\hbar\omega/k_{\mathrm{B}}T} - 1)^{-1}$ at frequency ω and temperature T. Because of the high optical carrier frequency (e.g., $\frac{\omega_{\mathrm{o}}}{2\pi} \sim 200$ THz for telecom light), we can safely assume $\bar{n}_{\mathrm{th,o}} \approx 0$ for optics even at room temperature. Therefore, in the following, we analyze only the environmental noise contributions from the microwave ($\bar{n}_{\mathrm{th,e}}$) and intermediate ($\bar{n}_{\mathrm{th,m}}$) thermal baths. Although the conversion efficiency is independent of the conversion direction because of the reciprocity of the linearized system, the environmental noise in general adds differently to the microwave and optical ports.

For zero-stage (direct) conversion, the added noise comes only from the microwave thermal bath. We have

$$n_{\mathrm{add(up)}} = \left(\frac{1}{\eta_{\mathrm{e}}} - 1\right)\bar{n}_{\mathrm{th,e}} \tag{7}$$

for microwave-to-optical conversion (upconversion) and

$$n_{\mathrm{add(down)}} = \frac{1-\eta_{\mathrm{e}}}{\eta_{\mathrm{o}}}\frac{1}{C_{\mathrm{eo}}}\bar{n}_{\mathrm{th,e}} \tag{8}$$

for optical-to-microwave conversion (downconversion). It can been seen that, besides a low operation temperature to directly reduce the environmental noise $\bar{n}_{\mathrm{th,e}}$, a very over-coupled microwave port ($\eta_{\mathrm{e}} \to 1$) can effectively suppress the added noise. This actually reveals the radiative cooling effect [39,40].

For one-stage conversion, in addition to the microwave noise, the thermal noise from the intermediate mode will also contribute to the total added noise ($n_{\mathrm{add}} = n_{\mathrm{add,m}} + n_{\mathrm{add,e}}$). The expressions are

$$n_{\mathrm{add,e(up)}} = \left(\frac{1}{\eta_{\mathrm{e}}} - 1\right)\bar{n}_{\mathrm{th,e}}, \tag{9}$$

$$n_{\mathrm{add,m(up)}} = \frac{1}{\eta_{\mathrm{e}}C_{\mathrm{em}}}\bar{n}_{\mathrm{th,m}} \tag{10}$$

for upconversion and

$$n_{\mathrm{add,e(down)}} = \frac{1-\eta_{\mathrm{e}}}{\eta_{\mathrm{o}}}\frac{(1+C_{\mathrm{om}})^2}{C_{\mathrm{om}}C_{\mathrm{em}}}\bar{n}_{\mathrm{th,e}}, \tag{11}$$

$$n_{\mathrm{add,m(down)}} = \frac{1}{\eta_{\mathrm{o}}C_{\mathrm{om}}}\bar{n}_{\mathrm{th,m}} \tag{12}$$

for downconversion. Similarly, the microwave added noise can be reduced by over-coupling the microwave port. But to suppress the intermediate mode noise, large cooperativities are also highly desired. Note that these noise expressions are generic and do not require the cooperativities to satisfy the matching conditions.

So far, we have focused on the special case with zero-detuning conversion (i.e., signal photons have the same frequency as cavity resonance). In practice, the signal to be converted is in a wave packet with a finite frequency range. It is important that all frequency components of the wave packet fall within the conversion band, which is limited by the rate of the slowest process of the conversion chain. For direct conversion, we may roughly estimate the conversion bandwidth as $B \sim (\kappa_{\mathrm{o}}^{-1} + \kappa_{\mathrm{e}}^{-1})^{-1} \sim \min[\kappa_{\mathrm{o}}, \kappa_{\mathrm{e}}]$. For one-stage conversion, the typical bandwidth is $B \sim \left(\kappa_{\mathrm{o}}^{-1} + \kappa_{\mathrm{e}}^{-1} + \frac{g_{\mathrm{em}}g_{\mathrm{om}}}{\sqrt{\kappa_{\mathrm{o}}\kappa_{\mathrm{e}}}}\right)^{-1} \sim \min\left[\kappa_{\mathrm{o}}, \kappa_{\mathrm{e}}, \frac{g_{\mathrm{em}}g_{\mathrm{om}}}{\sqrt{\kappa_{\mathrm{o}}\kappa_{\mathrm{e}}}}\right]$. For frequency conversion over a broad frequency range, it is desirable to have large external couplings and strong inter-mode couplings. The intermediate modes should also have sufficiently high frequencies to fulfill the resolved sideband condition.

4. INTRA-BAND QUANTUM FREQUENCY CONVERSION

A. Microwave-to-Microwave Frequency Conversion

In the microwave domain, the readily available, highly nonlinear Josephson junctions offering strong $\chi^{(2)}$ and $\chi^{(3)}$ microwave-to-microwave couplings, combined with the ultralow loss offered by superconductors, have enabled fully coherent frequency converters that reach conversion efficiency better than 99% [41–45] and added noise far below a quantum [39,40]. With a bandwidth exceeding 100 MHz and the ability to swap a quantum signal across beyond an octave, these devices are becoming common tools in quantum microwave circuits to couple resonators and qubits at dissimilar frequencies. Kinetic inductance nonlinear frequency converters, in the form of dispersion engineering transmission lines or nanowires, offer strong $\chi^{(3)}$ nonlinearity and will likely reach similar conversion performance and play an important role by offering an even larger conversion bandwidth and flexibility for spectral and temporal wave shaping [46]. The performance metrics demonstrated in superconductors provide a set of inspirational goals for M-O converters.

B. Optical-to-Optical Frequency Conversion

Frequency conversion of photonic states can be realized with nonlinear three- or four-wave mixing processes ($\chi^{(2)}$ or $\chi^{(3)}$) in bulk

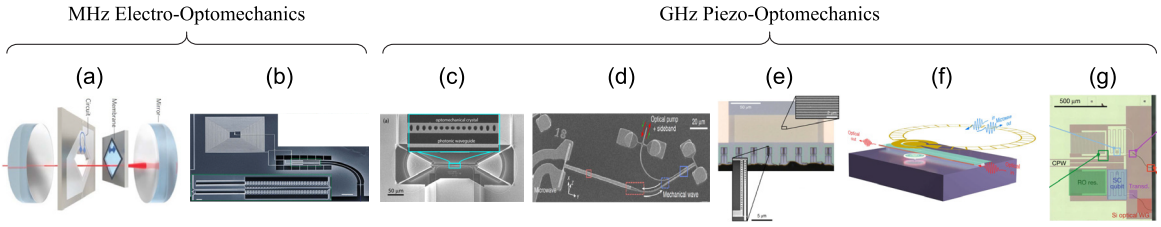

	(a)	(b)	(c)	(d)	(e)	(f)	(g)
$g_{om,0}$ [Hz]	6.6	0.66×10^6	115×10^3	80×10^3	1.3×10^6	19×10^3	$\sim 0.5 \times 10^6$
C_{om}	132	0.9	3×10^{-3}	5×10^{-3}	1.7	0.4	0.04
C_{em}	132	0.57	–	–	–	7	~ 150
η	0.47	1.9×10^{-4}	10^{-8}	10^{-5}	$< 3.5 \times 10^{-10}$	7.4×10^{-4}	8.8×10^{-6}
η_{in}	0.99	0.016	NR	0.026	NR	0.058	10^{-3}
$\frac{B}{2\pi}$ [MHz]	0.012	3.7×10^{-4}	~ 1	~ 1	NR	1	1
n_{add}	38	$\sim 10^4$	NR	NR	NR (∗)	NR	0.57 (∗∗)
T_{env} [K]	0.035	0.15	~ 300	~ 300	0.02	0.9	0.015

Fig. 3. MHz electro-optomechanical converters and GHz piezo-optomechanical converters [49–53]. (a) Membrane-based converter [38,47]. (b) Integrated MHz converter [48]. (c)–(e) Piezo-optomechanical crystal converters in AlN, LN, and GaAs [49–51], respectively. C_{em} is not applicable since microwave cavities are not involved in these designs. (f) Film thickness mode-based cavity piezo-optomechanical converter [52]. (g) Qubit-to-optical converter on AlN-on-Si platform [53]. The conversion uses a two-step pulsed protocol. NR, not reported; (∗), thermal occupancy of the mechanical mode is $\bar{n}_m = 0.9$; (∗∗), added noise referring to the qubit. (a),(e),(g) are reprinted by permission from Springer Nature [38,51,53] copyright 2014, 2020, 2020. (b),(d),(f) are reproduced from [48,50,52] under Creative Commons Attribution 4.0 International License. (c) is reprinted from Vainsencher *et al.*, Appl. Phys. Lett. 109. 033107 (2016) [49] with the permission of AIP Publishing.

crystals, nonlinear optical fibers, on-chip waveguides [54–57], as well as optomechanical crystals [58]. Because of the inherently weak photon–photon interactions, a strong parametric pump often is required to boost the frequency conversion efficiency in a $\chi^{(2)}$ process. (Two pumps are required for $\chi^{(3)}$ processes.) This robust pump could also initiate unwanted nonlinear optical processes, such as fluorescence and Raman scattering, which produce noise photons. In addition, the coupling between different optical components introduces inevitable optical losses. By leveraging integrated $\chi^{(2)}$ aluminum nitride (AlN)-on-insulator resonators at triple resonance conditions, bidirectional frequency conversion with 14% conversion efficiency and a bandwidth up to 1.2 GHz was demonstrated [59]. By using a periodically poled Ti-diffusion lithium niobate ($LiNbO_3$, LN) waveguide, up to 24% downconversion efficiency was realized [60]. However, significant efforts are needed to enhance the conversion efficiency and reduce the transducer noise to realize system efficiency beyond the 50% threshold required for non-classical quantum state transfer [61]. Recent developments of highly nonlinear, periodically poled thin film LN [62–64] and crystalline AlN thin film with ultralow Raman gain [65] point to promising routes for realizing photonic-chip-based efficient optical-to-optical photon converters.

5. CAVITY ELECTRO-OPTOMECHANICAL CONVERSION

Establishing efficient coupling between gigahertz microwave and telecom optical photons with five-orders-of-magnitude difference in frequency and wavelength is, in general, a very challenging task. One natural idea is to exploit an intermediate degree of freedom to mediate the interaction between microwave and optical photons. Phonons, which can be supported at microwave frequencies with their wavelength at the same scale as optical photons, stand out as an appealing candidate. During the past a few years, remarkable development in cavity optomechanics [66,67] and cavity electromechanics [68,69] has been accomplished especially in nanofabricated devices. Benefitting from these advancements, the hybrid electro-optomechanical photon conversion approach thus provides a very promising solution with encouraging recent progress.

A. MHz Electro-Optomechanics ($\chi^{(2)} \otimes \chi^{(2)}$)

By exploiting cavity-enhanced radiation pressure interaction at micro-/nano-scale, strong optomechanical interactions have been achieved at both optical [70,71] and microwave [72,73] frequencies. Successful combination of large optomechanical and electromechanical cooperativities in a hybrid device will lead to efficient M-O photon conversion.

The first realization of efficient bidirectional M-O photon conversion was demonstrated in a cavity electro-optomechanical system [38]. As shown in Fig. 3(a), the design implements a nanomembrane mechanical resonator to mediate the interaction between a 3D optical Fabry–Pérot cavity and a superconducting inductor-capacitor (LC) resonator. Made from silicon nitride with excellent optical and mechanical properties, the nanomembrane provides low-dissipation high-Q vibrational modes at $\sim$ MHz frequency [74,75] and cavity-enhanced optomechanical coupling with the optical cavity [70,76]. By partially coating the membrane with a thin layer of niobium (Nb) as a portion of the capacitor in the superconducting LC circuit, strong capacitive coupling ($\chi^{(2)}$) with the microwave resonator is simultaneously obtained.

The membrane-based converter design possesses several appealing advantages, in particular, for achieving large cooperativities and hence a high conversion efficiency. Compared with integrated photonic resonators that usually suffer from imperfect nanofabrication, the 3D optical cavity can easily offer higher Q ($Q_o > 10^8$) and lower dissipation rates $\left(\frac{\kappa_o}{2\pi} \sim 2\,\text{MHz}\right)$. Although the large mode volume gives only a small single-photon coupling rate $\left(\frac{g_{om,0}}{2\pi} \sim 10\,\text{Hz}\right)$, the bulk cavity can tolerate a very large amount

of pump photons ($n_{\mathrm{cav,o}} \sim 10^7$) to boost the optomechanical coupling rate to tens of kHz. Such a high-power optical pump is usually infeasible for on-chip converters, especially at cryogenic temperatures, due to the significant heat generation within a small device volume. A similar electromechanical coupling strength can be obtained under a microwave pump. Combined with the narrow mechanical linewidth ($\frac{\kappa_{\mathrm{m}}}{2\pi} \sim 10$ Hz) offered by the high-Q membrane resonator, large optomechanical and electromechanical cooperativities (C_{om}, $C_{\mathrm{em}} \gtrsim 100$) can be realized with the matching condition fulfilled via optical and microwave pump power adjustment.

The large cooperativities result in an almost perfect internal conversion efficiency $\eta_{\mathrm{in}} \approx 99\%$. Although highly over-coupled superconducting resonators are routinely exploited in experiments, it is a non-trivial technical challenge to achieve large over-coupling factor for the optical port without compromising the total optical linewidth or the optomechanical cooperativity. With further device optimization, an encouraging peak conversion efficiency of $\eta = 47\%$ (with $\eta_{\mathrm{o}} \sim 0.5$, $\eta_{\mathrm{e}} \sim 0.9$, and a bandwidth of 12 kHz) has been demonstrated in the membrane-based M-O converter [47]. This, so far, holds the efficiency record among all M-O photon conversion schemes, which is very close to the theoretical threshold of 50% required for quantum state transfer [61].

The challenge in MHz electro-mechanical systems, however, is the large thermal noise due to the low mechanical frequency. Although red-detuned pumps can induce a sideband cooling effect, which has been successfully exploited to cool MHz mechanical resonators to the quantum ground state [77,78], sufficiently low added noise ($n_{\mathrm{add}} < 1$) during photon conversion has not been realized yet. Combining the sideband cooling and a feed-forward protocol to harness noise correlations [47], the added noise of the membrane-based converter has been suppressed to $n_{\mathrm{add}} = 38$ operated at $T < 100$ mK temperatures. For quantum operations, the noise has to be further reduced to subphoton level.

It is worth mentioning that since MHz electro-mechanical systems systems are usually not fully within the resolved sideband regime (which requires $\omega_{\mathrm{m}} \gg \kappa_{\mathrm{o}}, \kappa_{\mathrm{e}}$), the two-mode squeezing interaction [$\hbar g_{\mathrm{om}}(a^\dagger m^\dagger + am)$ or $\hbar g_{\mathrm{em}}(b^\dagger m^\dagger + bm)$] from the optomechanical coupling cannot be completely neglected. This leads to a parametric amplification effect with a gain factor during the photon conversion. For example, a small gain factor about 1.3 is observed during the membrane-based photon conversion in Ref. [47], which, nevertheless, has been carefully calibrated out from the reported conversion efficiency. Although parametric amplification plays an essential role in many applications such as the development of quantum-limited amplifiers [45,79–82], it is not a noise-free process and at least half-photon added noise will be introduced (in the case of so called phase-preserving or phase-insensitive amplification) [83]. Therefore, throughout this review, we choose to discuss photon conversion efficiencies without any gain factors and the added noise refers to the input to better reveal features of different systems.

Recently, an integrated version of the cavity electro-optomechanical photon converter has been developed on a CMOS compatible silicon-on-insulator platform [48]. Compared with 3D free space cavities, on-chip converters offer great integratability and scalability. The design consists of an optomechanical photonic crystal zipper cavity with two aluminum coated nanostrings that are capacitively coupled to an on-chip superconducting LC resonator [Fig. 3(b)]. The large mode overlap and small mode volume of the optomechanical crystal produce a very large single-photon optomechanical coupling rate $\frac{g_{\mathrm{om},0}}{2\pi} \sim 0.7$ MHz. Despite the broader optical and mechanical linewidths from the nanofabricated resonators, the large $g_{\mathrm{om},0}$ substantially relaxes the required optical pump power; $C_{\mathrm{om}} \approx 0.9$ is obtained with an average pump photon number of only $\bar{n}_{\mathrm{cav,o}} \approx 0.2$ and pump power $P_{\mathrm{o}} = 625$pW. Further increase in pump power unfortunately causes severe heating and photon absorption effects in the nano-device, which degrade the quality factors and cooperativities. As a result, the highest on-chip conversion efficiency obtained is $\eta \approx 2 \times 10^{-4}$ at ∼150 mK, corresponding to an internal efficiency $\eta_{\mathrm{in}} \approx 1.6\%$, with $C_{\mathrm{em}} \approx 0.6$, $C_{\mathrm{om}} \approx 0.9$, and $\eta_{\mathrm{o}}\eta_{\mathrm{e}} \sim 0.01$. Note that because of the unresolved-sideband operation ($\kappa_{\mathrm{o}}/\omega_{\mathrm{m}} \sim 100$), Eq. (6) does not apply anymore, and a large parametric gain factor (∼ 100) has been separated out from the efficiency. The added noise is characterized to be $n_{\mathrm{add}} \approx 1.9 \times 10^4$ and 1.2×10^4 for the microwave-to-optical and optical-to-microwave conversion, respectively.

B. GHz Piezo-Optomechanics ($\chi^{(2)} \otimes \chi^{(1)}$)

Compared with low-frequency implementations, GHz mechanics offers a very attractive advantage in noise suppression. Because the thermal excitations are significantly reduced at high frequencies, GHz devices can automatically reach the quantum ground state ($\bar{n}_{\mathrm{th}} \ll 1$) at millikelvin temperatures via direct refrigeration [84–88] without the need of any active cooling techniques such as laser cooling.

Operated at the same microwave frequencies, GHz mechanical devices may directly couple with superconducting quantum circuits via the linear piezoelectric effect ($\chi^{(1)}$). Although capacitive coupling could still be employed under a DC bias [89], piezoelectric coupling permits contactless coupling configurations [90,91] without the need for metal deposition on the mechanical objects and microwave pump tones, which is convenient especially in the presence of optical components. Moreover, piezoelectric coupling can be very strong; electromechanical strong coupling with large cooperativities ($C_{\mathrm{em}} > 2000$) has been demonstrated in superconducting piezomechanical systems [91]. With further integration of superconducting qubits, control and manipulation of phonon quantum states at GHz frequencies have been demonstrated in several recent remarkable experiments [84,92–96].

Realizations of high-frequency GHz cavity optomechanics include optomechanical crystals [49,51,97–102], thickness mode-based thin-film resonators [90,103,104], Brillouin-scattering cavities [105,106], and high-overtone bulk acoustic resonators [107–109]. Aiming for efficient photon conversion, optomechanical crystals are very attractive due to their large single-photon optomechanical coupling rate. By engineering periodic structures in a suspended nanobeam, photonic and phononic bandgaps can be created simultaneously to confine optical light and mechanical vibrations at ∼μm scale in an optomechanical crystal. The maximized mode overlap within a minimized mode volume results in very large single-photon coupling rates ($\frac{g_{\mathrm{om},0}}{2\pi} \sim$ MHz).

Fabricating optomechanical crystals in piezoelectric materials would allow strong electromechanical interaction for M-O photon conversion. Choices of material platforms include gallium arsenide (GaAs), AlN, and LN. GaAs has a weaker piezoelectric effect compared with AlN and LN (piezoelectric coefficients: $e_{14,\mathrm{GaAs}} = -0.16\mathrm{C/m}^2$, $e_{33,\mathrm{AlN}} = 1.55\mathrm{C/m}^2$, $e_{14,\mathrm{LN}} = 1.77\mathrm{C/m}^2$). But larger optomechanical coupling

($\frac{g_{om,0}}{2\pi} \sim 1$ MHz) can be obtained in GaAs [100,101] due to the stronger photoelastic effect, and $\frac{g_{om,0}}{2\pi} \sim 100$ kHz for AlN [49] or LN [50,102] piezo-optomechanical crystals.

To couple a microwave with mechanical motions, non-resonant transducers such as metal electrodes and interdigital transducers (IDTs) have been widely implemented for studying the coherent transduction from microwave to optics [101,110]. Without a microwave resonator, the photon conversion efficiency should no longer be described by Eq. (6). Instead, the electromechanical transduction can be represented by a single efficiency factor η_{em}, and the total photon conversion efficiency reduces to a "direct-conversion" form:

$$\eta = \eta_{em}\eta_o \frac{4C_{om}}{(1+C_{om})^2}. \tag{13}$$

Integrating IDTs at the far ends of a 3.8-GHz AlN piezo-optomechanical crystal [Fig. 3(c)], bidirectional M-O photon conversion at room temperature has been observed with a total efficiency $\eta \sim 10^{-8}$ [49]. Recently, a higher efficiency of $\eta \sim 10^{-5}$ at room temperature has been achieved in a 1.8-GHz LN device [Fig. 3(d)] with $\eta_{em} \sim 10^{-3}$, $\eta_o \sim 0.7$, and $C_{om} \sim 0.01$ [50].

The low-noise advantage of GHz devices has been revealed in a 2.7-GHz GaAs optomechanical crystal [Fig. 3(e)] at ~20 mK [51]. Using a pulsed laser pump scheme to reduce heating effects, coherent microwave-to-optical photon conversion has been observed while maintaining the mechanical mode close to its quantum ground state ($\bar{n}_m \approx 0.9$). A large cooperativity of $C_{om} \approx 1.7$ is obtained with a pump photon number $n_{cav,o} = 280$, which provides efficient internal conversion between phonons and optical photons. The overall photon conversion efficiency, however, is significantly limited by the low electromechanical transduction factor $\eta_{em} \sim 10^{-10}$, and the added noise is presumably large when referring to the input.

Without cavity-enhanced coupling, efficient electromechanical transduction ($\eta_{em} \to 1$) can be hardly achieved. Because of the large impedance mismatch, IDTs typically experience more than 20-dB loss when transferring spatially broad surface acoustic waves into a nanobeam resonator. Further improvement of acoustic transducer efficiency is expected by leveraging the design concepts developed by the broader microelectromechanical system (MEMS) community. A capacitively coupled LC resonator has been recently integrated with a MHz optomechanical crystal [48]; however, similar schemes have to be implemented in GHz piezo-optomechanical crystal converters with sufficient electromechanical coupling. Feasible device parameters have been recently analyzed in theory, and a mechanical "supermode" design has been proposed by extending the highly localized mechanical mode for interfacing with an impedance-matched LC circuit [111]. Combining the circuit resonator and the best performance in GHz optomechanical crystals [112,113], it is estimated that high conversion efficiency ($\eta > 99\%$) and low added noise ($n_{add} < 0.1$) are simultaneously achievable using a hybrid AlN-on-Si device.

Another promising implementation for efficient high-frequency piezo-optomechanical M-O conversion is to exploit the thickness mode-based optomechanical resonators. By harnessing the fundamental acoustic standing-wave modes across the thickness of thin films, high-frequency mechanical resonances at ~10 GHz have been realized in AlN micro-wheels [90] and micro-disks [103]. At the same time, high-Q optical whispering-gallery modes are supported in these micro-resonators, providing optomechanical coupling. Compared with optomechanical crystals, the relatively large mode volume (typically a few micron in radius) of thickness mode-based resonators results in a smaller single-photon coupling rate ($\frac{g_{om,0}}{2\pi} \sim 10$ kHz) [52,103]. Nevertheless, the larger area of these thin-film structures makes it convenient to strongly couple with superconducting resonators through the piezoelectric effect.

By integrating a planar niobium nitride (NbN) superconducting resonator over a 10-GHz AlN optomechanical micro-disk [Fig. 3(f)], the first cavity piezo-optomechanical photon converter has been recently demonstrated [52]. Because of the superconducting cavity enhancement, a large piezo-electromechanical cooperativity of $C_{em} \sim 7$ was realized. With the implementation of a pulsed optical pump scheme for boosting the intracavity photon number ($n_{cav} \sim 10^5$), an optomechanical cooperativity of $C_{om} \sim 0.4$ was achieved, leading to a significantly improved internal efficiency $\eta_{in} \approx 5.8\%$ and an on-chip efficiency $\eta_{in} \approx 10^{-3}$ over a 1-MHz conversion bandwidth. The device was operated at ~1 K for better power handling and heat dissipation, where the environmental thermal noise was expected to be a few photons at 10 GHz. With further incorporation of the radiative cooling technique [39,40] to suppress thermal noise via the microwave cooling channel to millikelvin, realization of subphoton added noise could be promising.

Recently, GHz piezo-optomechanics has been directly integrated with a superconducting qubit to realize an impressive demonstration of transduction from qubit quantum excitations to optical photons [53]. As shown in Fig. 3(g), the device was fabricated on a hybrid AlN-on-Si platform where the microwave field of a transmon qubit is piezoelectrically coupled to the GHz phonon modes of a Si optomechanical crystal through an IDT capacitor on top of the AlN layer. The qubit-to-optical conversion was achieved using a two-stage protocol in pulse mode. Qubit excitations were first swapped to phonons by tuning the qubit frequency into and out of the mechanical resonance using the a.c. Stark shift. Due to the strong piezoelectric coupling, a high single-phonon initialization probability of 75% was achieved. Then by applying a red-detuned pump laser pulse, phonons are coherently transduced to optical photons through the optomechanical crystal. By detecting the converted photons using single-photon detectors, quantum Rabi oscillation of the qubit was successfully recorded optically. The experiments were conducted under a low-power pump ($n_{cav,o} = 44$) to avoid excessive heating and noise, and an internal qubit-to-optical conversion efficiency of $\eta_{in} \approx 10^{-3}$ with subphoton added noise (referring to the qubit) $n_{add} \approx 0.6$ was achieved at 15 mK. The overall system efficiency was measured to be $\sim 10^{-5}$ when taking into account all the optical readout loss.

6. CAVITY ELECTRO-OPTIC CONVERSION ($\chi^{(2)}$)

Recently, cavity electro-optics [114–122] has attracted great attention as a promising route toward efficient and low-noise M-O photon conversion. Unlike other schemes that utilize intermediate modes, electro-optic devices employ the Pockels effect ($\chi^{(2)}$)—changing the optical refractive index by the electric field—to directly interface optical and microwave signals. Without relying on free-standing structures, electro-optic schemes offer low fabrication complexity with excellent scalability and power handling capability. By positioning an optical cavity made from Pockels materials in the electric field of a microwave resonator, the optical

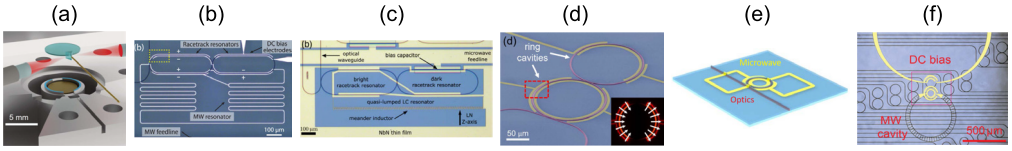

	(a)	(b)	(c)	(d)	(e)	(f)
$\frac{g_{eo,0}}{2\pi}$ [Hz]	36	1200	650	750	310	42
C_{eo}	1.7×10^{-3}	NR	NR	0.041	0.075	3×10^{-4}
η	3.16×10^{-4} (2.3×10^{-7})	6.6×10^{-6}	2.7×10^{-5}	0.01	0.02	2.4×10^{-5} ($\sim 3.3 \times 10^{-6}$)
η_{in}	6.7×10^{-3} ($\sim 5 \times 10^{-6}$)	NR	NR	0.152	0.259	0.0012 (NR)
$\frac{B}{2\pi}$ [MHz]	9	20	13	NR	0.59	2.9
n_{add}	$5.5/\eta$ ($0.03/\eta$)	NR	NR	NR	NR	NR (∗) (NR (∗))
T_{env} [K]	0.32 (0.007)	1	1	1.9	2	∼0.15 (0.04)

Fig. 4. Cavity electro-optic converters. (a) Bulk LN 3D cavity converter [123,124]. (b)–(d) Integrated LN converters [114–116], respectively. (e),(f) Integrated AlN converters [117,118]. NR, not reported; (∗), thermal occupancy of the microwave mode is $\bar{n}_e = 1.8$ ($\bar{n}_e = 0.09$). (a) and (f) are reprinted with permission from [124] and [118] Copyright (2020) and (2021) by the American Physical Society. (b) and (c) are reprinted from [114,115] under terms of The Optical Society-Open Access Agreement. (d) and (e) are reprinted from [116] and [117] under terms of the Creative Commons Attribution-NonCommercial license.

and microwave modes can be coupled via the electro-optic effect, providing strong three-wave-mixing nonlinearity for direct M-O photon conversion.

To obtain a high electro-optical coupling rate, besides choosing materials with large intrinsic $\chi^{(2)}$ coefficients, careful device design and engineering are also required to maximize the mode overlap and minimize mode volumes. In addition, to boost g_{eo}, a second optical mode is routinely employed to enhance the intracavity pump photon number. With the pump mode, pump photons can much more efficiently couple into the cavity, especially in the resolved-sideband regime where the pump frequency is detuned out of the cavity resonance. The pump and signal optical modes can be engineered via various approaches including using optical modes that are one free spectral range (FSR) apart [123,124], or modes with orthogonal polarizations [117], or hybridized modes in two coupled rings [114–116,118]. Importantly, the pump mode, optical cavity mode, and microwave mode have to fulfill the phase matching condition: the frequency and azimuthal number differences of the two optical modes need to match those of the microwave mode, respectively.

Due to its large electro-optic coefficient ($r_{33} = 31$ pm/V), LN stands out as one of the most appealing materials for electro-optic converters. High-Q optical whispering-gallery-mode resonators ($Q_o \sim 10^8$) have been made from bulk LN in millimeter size. By placing the LN resonator in a 3D microwave cavity [Fig. 4(a)], coherent M-O photon conversion has been achieved [123,124] with a total (internal) efficiency up to 3.16×10^{-4} ($\eta_{in} \approx 0.67\%$) and a bandwidth of 9 MHz operated at cryogenic temperature. The large optical and microwave mode volumes lead to a small single-photon coupling rate $\frac{g_{eo,0}}{2\pi} \approx 36$ Hz, which gives an electro-optic cooperativity $C_{eo} \approx 1.7 \times 10^{-3}$ under an optical pump power of 1.48 mW ($n_{cav,o} \sim 10^8$). The noise at the output port is measured to be $n_{out} \approx 5.5$ photons, corresponding to an added noise of $n_{add} \sim 10^4$ when referring to the input. As a GHz converter that can automatically reach quantum ground state at ∼mK temperature, lower output noise ($n_{out} \approx 0.03$) and a ground-state microwave mode occupancy ($\bar{n}_e \approx 0.025 \ll 1$) have been observed with reduced pump power, which sacrifices the total conversion efficiency down to 2.3×10^{-7} at the same time.

With recent advancement in LN nanofabrication techniques [125,126], the electro-optic coupling strength can be substantially improved in on-chip devices with minimized mode volumes at micro-scale. By integrating LN micro-ring optical resonators with on-chip superconducting microwave LC resonators [Figs. 4(b)–4(d)], recent implementations of integrated LN electro-optic M-O photon converters [114–116] have demonstrated larger single-photon coupling rates up to $\frac{g_{eo,0}}{2\pi} \sim 1$ kHz, and an improved total (internal) conversion efficiency of $\eta \approx 1\%$ ($\eta_{in} \approx 15\%$) has been achieved using a pulsed optical pump scheme [116]. Despite challenges such as the photo-refractive effect and optically induced charge [127] that remain to be alleviated, LN-based electro-optic converters show great potential for efficient and low-noise M-O photon conversion.

Another excellent material platform for electro-optic conversion is AlN. Although AlN has a smaller electro-optic coefficient ($r_{13} = 1$ pm/V) compared with LN, AlN devices are easier to process without suffering from the photo-refractive effect or optically induced charge. With careful device design and engineering [Fig. 4(e)], a single-photon electro-optic coupling rate of $\frac{g_{eo,0}}{2\pi} \approx 300$ Hz has been demonstrated [117] in a fully integrated AlN device. By immersing the device in superfluid helium at 2 K for better heat dissipation, a large number of pump photons ($n_{cav,o} \approx 3 \times 10^7$) was applied to enhance the electro-optic cooperativity to $C_{oe} \approx 0.075$, resulting in an on-chip (internal) photon conversion efficiency of $\eta \approx 2\%$ ($\eta_{in} \approx 25\%$) with a bandwidth of 0.59 MHz. The added noise was estimated to be $n_{add} \sim 3$ without experimental characterization.

Toward further reduction of added noise to below subphoton level for quantum operations, M-O photon conversion using an integrated AlN cavity electro-optic circuit in the quantum ground state has been recently observed [118]. The device implements a flip-chip bonding technique to integrate an AlN micro-ring resonator with a NbN superconducting resonator fabricated on separate chips [Fig. 4(f)], obtaining a single-photon coupling rate of $\frac{g_{eo,0}}{2\pi} \approx 42$ Hz. By operating the device in a 40-mK environment

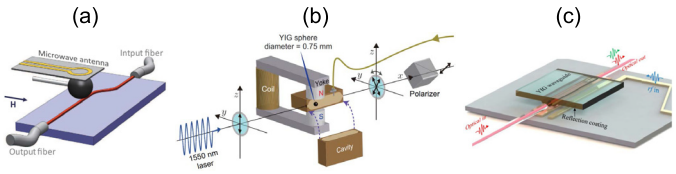

$\frac{g_{\mathrm{mago},0}}{2\pi}$	[Hz]	0.33	3.3×10^{-4}	17.2
$\frac{C_{\mathrm{mago}}}{2\pi}$	[Hz]	5.4×10^{-10}	–	4.06×10^{-7}
$\frac{C_{\mathrm{mage}}}{2\pi}$	[Hz]	–	510	0.8
η		1.7×10^{-15}	10^{-10}	1.08×10^{-8}
η_{in}		6×10^{-6}	NR	5.19×10^{-7}
$\frac{B}{2\pi}$	[MHz]	NR	NR	16.1
T_{env}	[K]	~ 300	~ 300	~ 300

Fig. 5. Magnon-mediated converters. (a) Cavity optomagnonics in a YIG sphere. C_{mage} is not applicable since no microwave cavity is involved [128,129]. (b) YIG sphere-based converter. C_{mago} is not applicable since no optical cavity is involved [130]. (c) Integrated cavity optomagnonic waveguide converter. NR, not reported [131,132]. (a) and (b) are reprinted with permission from [128] and [130] Copyright (2016, 2016) by the American Physical Society. (c) is reproduced from 131 under terms of The Optical Society-Open Access Agreement.

with a pulsed optical pump scheme, an on-chip photon conversion efficiency of $\eta \approx 3.3 \times 10^{-6}$ has been achieved while maintaining the microwave mode close to quantum ground state (microwave mode occupancy $\bar{n}_{\mathrm{e}} \approx 0.09$). Unlike the converter based on polycrystalline AlN sputtered on thermal oxide in Ref. [117], this work utilizes crystalline AlN thin films epitaxially grown on sapphire substrates, which promise lower optical and dielectric losses for heterogeneous superconducting photonic device integration.

7. MAGNON-MEDIATED CONVERSION ($\chi^{(2)} \otimes \chi^{(1)}$)

Another attractive candidate for mediating the M-O photon interaction is magnon—the collective excitation of spins in magnetically ordered materials. The exploration of magnon-mediated M-O photon conversion is highly motivated by the large tunability and broad bandwidth offered in magnetic devices. In particular, yttrium iron garnet (YIG), as a ferrimagnetic insulator, attracts great attention because of its excellent low-dissipation property for all types of carriers in spin waves, acoustics, microwave, and optics. Moreover, as quanta of perturbation in spin ordering, magnons can easily interact with microwave photons through the linear magnetic dipole interaction ($\chi^{(1)}$). Strong coupling [133–135] and even ultrastrong coupling [136] between magnons and microwave cavity photons has been demonstrated in YIG devices.

To interconvert magnons and optical photons, the magneto-optical coupling can be achieved via the Faraday or inverse Faraday effect, which is effectively a three-wave-mixing ($\chi^{(2)}$) process that can be described by a Hamiltonian similar to that of optomechanical interaction. But the difference is that the annihilation and creation of magnons are accompanied with the change in optical photon polarization due to the conservation of angular momentum. Such coherent conversion between magnons and optical photons has been successfully observed in YIG sphere resonators [128–130,137], where the uniform magnon mode (Kittel mode) [138] is harnessed to interact with guided whispering-gallery optical modes [Fig. 5(a)]. By coupling a YIG sphere with a 3D microwave cavity [Fig. 5(b)], bidirectional M-O photon conversion has been observed at room temperature [130]. However, because of the large volume of YIG spheres (typically a few hundreds of micrometers in diameter), the achievable magneto-optical coupling is very limited ($\frac{g_{\mathrm{mago},0}}{2\pi} \lesssim 1$ Hz and $C_{\mathrm{mago}} \lesssim 10^{-9}$) even with optical cavity enhancement [128,129,137], which remains a major bottleneck for efficient M-O photon conversion.

Despite the extreme difficulty in YIG nanofabrication, recent efforts have successfully demonstrated an on-chip optomagnonic waveguide resonator [Fig. 5(c)] in a single crystalline YIG thin film [131,132]. The waveguide resonator simultaneously supports multiple forward volume magnetostatic standing wave (FVMSW) magnon modes and optical Fabry–Pérot resonances with significantly reduced mode volume and increased mode overlap. As a result, the single-photon magneto-optical coupling is improved to $\frac{g_{\mathrm{mago},0}}{2\pi} \approx 17$ Hz with a cooperativity of $C_{\mathrm{mago}} \approx 4 \times 10^{-7}$ under a pump photon number $n_{\mathrm{cav,o}} \sim 10^6$ at room temperature. With an integrated half-lambda microwave resonator for strong magnon–microwave coupling, M-O photon conversion was observed in both directions with an on-chip efficiency $\eta \approx 10^{-8}$ and an internal efficiency $\eta_{\mathrm{in}} \approx 5 \times 10^{-7}$. A broad conversion bandwidth over 16 MHz was obtained due to the multimode magnon resonances.

8. ATOM-ASSISTED CONVERSION ($\chi^{(2)}$, $\chi^{(5)}$, $\cdots$)

Atom-assisted M-O photon conversion is an appealing approach that can conveniently incorporate various existing quantum technologies based on atoms and solid-state emitters [139]. These emitters provide effective nonlinearity for mixing optical and microwave fields through a closed loop of transitions. For instance, as shown in Fig. 6(a), by selecting two near-degenerate hyperfine energy levels ($|1\rangle$, $|2\rangle$) for ground states and an optical excited state ($|3\rangle$), a three-wave mixing process can be realized through the transitions $|1\rangle \rightarrow |2\rangle \rightarrow |3\rangle \rightarrow |1\rangle$. Then, coherent conversion between optical (a) and microwave (b) photons can be realized under an optical drive (Ω) close to electronic resonance ($|2\rangle \leftrightarrow |3\rangle$). Such three-wave mixing manifests an effective $\chi^{(2)}$ nonlinearity similar to the electro-optic or magneto-optic effects, with an effective $\chi^{(2)}$ coefficient greatly enhanced by the near-resonance transitions and large optical depth due to the high atomic density when compared with intrinsic nonlinearity of dielectrics.

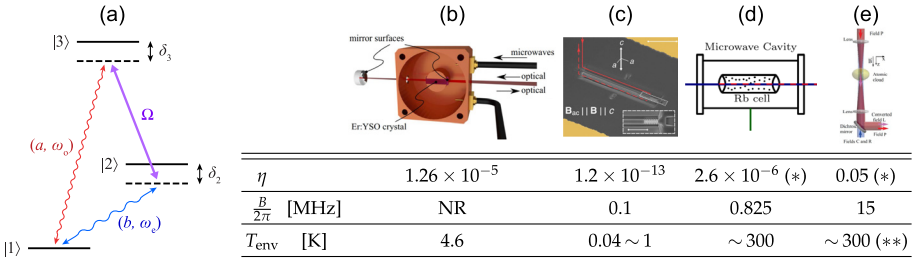

η		1.26×10^{-5}	1.2×10^{-13}	2.6×10^{-6} (∗)	0.05 (∗)
$\frac{B}{2\pi}$	[MHz]	NR	0.1	0.825	15
T_{env}	[K]	4.6	$0.04 \sim 1$	~ 300	~ 300 (∗∗)

Fig. 6. (a) Schematic of a three-level system illustrating atom-assisted microwave-optical photon conversion. (b) Converter based on bulk Er^{3+}:YSO crystal [140,141]. (c) Integrated converter based on a $^{171}Yb^{3+}$:YVO_4 nanophotonic waveguide [142]. (d) Microwave-to-near-infrared converter using a ^{85}Rb hot atom vapor cell [143]. (e) Cold ^{87}Rb ensemble-assisted converter between 84.18-GHz microwave and 780-nm optical fields [144]. NR, not reported; (∗), efficiency is calculated as the converted optical photon number divided by the number of input microwave photons incident on the cross section of the atom cloud; (∗∗), the atom cloud is cooled to ~ 70 μK using a magneto-optical trap. (b) and (e) are reprinted with permission from [141] and [144] Copyright (2019, 2019) by the American Physical Society, (c) is reprinted from [142] under a Creative Commons Attribution 4.0 International License. (d) is reprinted with permission from [143] © The Optical Society.

Various emitters in solids with addressable transitions in both optical and microwave regimes, such as the NV center [145,146] and rare-earth ions (REI) [140–142,147–149], have been explored for M-O conversion. Among these systems, REI ensembles have attracted particular attention with recent promising progress. First proposals of REI-based transducers [147,148] suggest using erbium-doped yttrium orthosilicate (Er^{3+}:YSO) crystals to mediate the interaction between optical and microwave fields. Er^{3+} ions have many attractive advantages: their optical transition $^4I_{15/2} \leftrightarrow {}^4I_{13/2}$ is in the telecommunications band, and the transition has narrow inhomogeneous and homogeneous linewidths. By applying an external magnetic field, the degenerate ground state doublets are split into two states ($|1\rangle$ and $|2\rangle$). Therefore, with a common excited state ($|3\rangle$), the ions exhibit three energy levels that have both optical and microwave transitions, and the microwave transition frequency can be tuned by the external magnetic field. Considering the inhomogeneous broadening of transitions, the optical and microwave modes should be detuned from the transition frequencies by more than the inhomogeneous linewidth to adiabatically eliminate the atom dynamics and preserve phase coherence. The detuning inevitably decreases the coupling strength; therefore, it is essential to have the product of optical and microwave cooperativity factors larger than one to achieve efficient conversion [148].

Experimentally, the scheme is first realized by using a 3D copper microwave cavity to couple a single-passed optical field via Er^{3+}:YSO crystal [Fig. 6(b)]. Upconversion is demonstrated with the conversion efficiency estimated to be $\sim 10^{-12}$ [140]. Later, using a Fabry–Perot resonator to enhance the optical field, the conversion efficiency was improved to 1.26×10^{-5} [141]. Further improvement could come from better impedance matching and a lower-temperature environment, where ions are cooled to the ground state and dephasing mechanisms are reduced. In addition, fully concentrated REI crystals with high rare-earth concentrations and low optical and microwave inhomogeneous linewidths were proposed to improve the M-O photon conversion performance [149]. The first integrated REI converter has been recently reported by harnessing $^{171}Yb^{3+}$-doped yttrium orthovanadate (YVO_4) crystals [142]. The converter consists of a $^{171}Yb^{3+}$:YVO_4 nanophotonic waveguide, where the REI ensemble is coupled to the microwave field generated by a gold coplanar waveguide [Fig. 6(c)]. The energy levels of $^{171}Yb^{3+}$ allow coherent M-O photon conversion at near-zero and zero magnetic field, which is beneficial for integrating other quantum devices such as superconducting qubits. Using this device, microwave-to-optical photon conversion is observed with an efficiency of 1.2×10^{-13} and a bandwidth of 100 kHz. Improvement in efficiency could be accomplished by using cavities to enhance the spin–photon interactions at both optical and microwave frequencies.

The scheme shown in Fig. 6(a) could also be easily implemented in hot and cold atom gases [150,151]. Distinct from solid-state systems, atomic gases are compatible with optical transitions over a huge wavelength span, ranging from ultraviolet to intermediate infrared wavelengths, and also feasible for interfacing abundant microwave transitions ranging from GHz to hundreds of GHz by employing the high-lying Rydberg energy levels. Benefitting from large electric dipole moments of Rydberg states, an internal conversion efficiency of over 90% is predicted in theoretical proposals for bidirectional M-O photon conversion in Rydberg atoms [152,153].

The coherent frequency conversion from ∼3-GHz microwave to near-infrared (795 nm) optical field is demonstrated using a ^{85}Rb hot atom vapor cell at room temperature [Fig. 6(d)] with a bandwidth of 825 kHz and an efficiency of 2.6×10^{-6} [143]. Recently, a proof-of-principle experiment was carried out in a cold ^{87}Rb ensemble [Fig. 6(e)] via a six-wave mixing ($\chi^{(5)}$) process employing closed-loop transitions of six energy levels, demonstrating a conversion efficiency of ∼5% between 84.18-GHz microwave and 780-nm optical fields, with a bandwidth of about 15 MHz [144,154]. The experimental system holds the potential for realizing 70% conversion efficiency in an optimized configuration. It is worth pointing out that in the atom gas-assisted approaches, the conversion efficiency is typically calculated by considering only the input microwave photons incident on the cross section of the atom cloud, which is different from our definition of η and η_{in}.

The M-O photon conversion schemes exploiting long-coherence-time ground hyperfine energy levels in atoms could also be treated as a continuous operation of quantum memory, which stores microwave signals to collective spin excitations in the atomic ensemble and retrieves the signals to optical photons. Therefore, ultrahigh-fidelity quantum memories demonstrated in cold-atom ensembles [155] could indicate very high M-O conversion efficiency that is worth further experimental efforts.

9. OUTLOOK OF QUANTUM TRANSDUCTION

Quantum transduction across different platforms will undoubtedly become a key technology in the revolutionary development of quantum science. The realization of M-O quantum converters will not only enable quantum state transfer between the microwave and optics, but also create essential capabilities, such as optical quantum repeaters based on microwave quantum control and error correction, and distributed superconducting quantum computing via optical quantum links. Although quantum-enabled M-O converters are yet to be demonstrated, the above-discussed efforts and progress have certainly been very encouraging.

Toward high-efficiency and low-noise M-O photon conversion, how to achieve large cooperativities with moderate pump power while maintaining the sufficiently low mode temperature (∼mK) required for microwave quantum operations still remains a significant challenge. Possible solutions include better material and device engineering for stronger single-photon nonlinearity and lower loss, and/or improved heat dissipation techniques such as the use of all epitaxial photonic and superconducting films [156,157], radiative cooling [39,40], and superfluid cooling [117]. In addition, a large conversion bandwidth is highly desired for transferring quantum information, which is inevitably limited by the resonance linewidth of cavity converters. Broadband conversion could be realized via multimode systems such as optoelectromechanical arrays [158] or continuum optomechanics with Brillouin scattering [159].

So far, what we have discussed can be classified as direct quantum transduction (DQT), which simply injects quantum signals to the input port and retrieves them from the output port of the converter. Because quantum signals are vulnerable to both attenuation and amplification, DQT has stringent efficiency and noise requirements. Devices developed for DQT can be exploited in alternative quantum transduction protocols, which, including adaptive quantum transduction (AQT) and entanglement-based quantum transduction (EQT), have been explored to possibly bypass the demanding requirements of DQT.

The AQT protocol [33] prepares a squeezed vacuum as an ancilla input for the converter, then performs homodyne detection at the idler port and applies adaptive control to the output conditioned on the homodyne measurement results. In this way, by harnessing the noise correlation created by the squeezed vacuum ancilla, added noise at the output port can be canceled, and signal leakage to the environment can be prevented, hence relaxing the quantum state transfer requirements of DQT. The EQT protocol [35,160] generates entangled M-O photon pairs and then uses them to perform quantum teleportation for quantum state transfer. This protocol uses additional classical signaling of intermediate measurement outcomes and can bypass the efficiency threshold for quantum channel capacity in DQT protocols. Time-bin [35] or frequency-bin [161] encoding can be implemented to verify the M-O entanglement in the presence of practical imperfections due to excitation loss and thermal noises.

The above-mentioned quantum transduction protocols are fully compatible with recent experiments, and can be generalized to different types of M-O photon converters. Combining these encouraging and remarkable developments in both theory and experiment, quantum state transfer between the microwave and optics could be soon within reach in the near future, enabling unprecedented advantages in quantum computing, quantum sensing, and quantum communication.

APPENDIX A: COEFFICIENT MATRICES FOR MULTI-STAGE CONVERSION

In the general case of N-stage M-O photon conversion, the coefficient matrices of the Heisenberg equation of motion have the following forms:

$$\mathbf{A}=\begin{pmatrix} \Gamma_{\mathrm{o}} & ig_{\mathrm{om}} & 0 & \cdots & & 0 \\ ig_{\mathrm{om}} & \Gamma_{\mathrm{m1}} & ig_{12} & & & \\ 0 & ig_{12} & \Gamma_{\mathrm{m2}} & \ddots & & \vdots \\ & \ddots & \ddots & \ddots & & \\ \vdots & & \ddots & \Gamma_{\mathrm{m}(N-1)} & ig_{(N-1)N} & 0 \\ & & & ig_{(N-1)N} & \Gamma_{\mathrm{m}N} & ig_{\mathrm{em}} \\ 0 & \cdots & & 0 & ig_{\mathrm{em}} & \Gamma_{\mathrm{e}} \end{pmatrix}, \tag{A1}$$

$$\mathbf{B}=\begin{pmatrix} \sqrt{\kappa_{\mathrm{o,ext}}} & \sqrt{\kappa_{\mathrm{o,int}}} & 0 & \cdots & & 0 \\ 0 & 0 & \sqrt{\kappa_{\mathrm{m1}}} & & & \\ \vdots & & & \ddots & & \vdots \\ & & & & \sqrt{\kappa_{\mathrm{m}N}} & 0 \\ 0 & & \cdots & & 0 & \sqrt{\kappa_{\mathrm{e,ext}}} \quad \sqrt{\kappa_{\mathrm{e,int}}} \end{pmatrix}. \tag{A2}$$

Here, $\Gamma_{\mathrm{o}} \equiv -i(\omega_{\mathrm{o}}-\omega_{\mathrm{p,o}})-\frac{\kappa_{\mathrm{o}}}{2}$, $\Gamma_{\mathrm{e}} \equiv -i(\omega_{\mathrm{e}}-\omega_{\mathrm{p,e}})-\frac{\kappa_{\mathrm{e}}}{2}$, and $\Gamma_{\mathrm{m}j} \equiv -i\omega_{\mathrm{m}j}-\frac{\kappa_{\mathrm{m}j}}{2}$. $\omega_{\mathrm{p,o}}$ and $\omega_{\mathrm{p,e}}$ denote the optical and microwave parametric pump frequencies, respectively. The terms $(\omega_{\mathrm{o}}-\omega_{\mathrm{p,o}})$ and $(\omega_{\mathrm{e}}-\omega_{\mathrm{p,e}})$ can be viewed as the cavity resonant frequencies in the pump rotating frames. In the case of linear ($\chi^{(1)}$) interaction such as piezoelectric coupling, one can simply set $\omega_{\mathrm{p,e}}=0$.

Plugging **A** and **B** matrices into Eq. (4), one can obtain the complete expression of the scattering matrix. For example, the M-O photon conversion spectrum is given by $\eta[\omega]=|\mathbf{S}_{1,(N+3)}|^2=|\mathbf{S}_{(N+3),1}|^2$. In the case when all the modes share the same resonant frequency (i.e., $\omega_{\mathrm{m}j}\equiv\omega_{\mathrm{m}}$, and the pumps are red-detuned by $\omega_{\mathrm{o,p}}-\omega_{\mathrm{o}}=\omega_{\mathrm{e,p}}-\omega_{\mathrm{e}}=-\omega_{\mathrm{m}}$), the conversion efficiency at zero-detuning ($\omega=\omega_{\mathrm{m}}$) can be expressed in simple forms of cooperativities as shown in Eqs. (5) and (6). The conversion bandwidth and noise performance can also be obtained from the scattering matrix. For example, the microwave added noise for upconversion can be calculated from the output noise $|\mathbf{S}_{1,(N+4)}|^2\bar{n}_{\mathrm{th,e}}$ divided by the conversion efficiency η.

Funding. Army Research Office (W911NF-18-1-0020); Air Force Office of Scientific Research (FA9550-15-1-0015, FA9550-15-1-0029); David and Lucile Packard Foundation (2013-39273); National Science Foundation (EFMA-1640959); Office of Science (DE-AC02-06CH11357).

Acknowledgment. LJ acknowledges supports from AFOSR MURI and the Packard Foundation. HXT acknowledges supports from AFOSR MURI and NSF EFRI. XH's work was performed, in part, at the Center for Nanoscale Materials, a U.S. Department of Energy Office of Science User Facility, and supported by the U.S. Department of Energy, Office of Science. The authors thank M. H. Devoret, S. Shankar, M. Xu, M. Zhang, C. Zhong, C.-H. Wang, S. Chowdhury, Z. Wang, N. Zhu, X. Zhang, L. Yang, and Y. Xu for valuable discussions.

Disclosures. The authors declare no conflicts of interest.

REFERENCES

1. B. B. Blinov, D. L. Moehring, L.-M. Duan, and C. Monroe, "Observation of entanglement between a single trapped atom and a single photon," Nature **428**, 153–157 (2004).

2. D. N. Matsukevich and A. Kuzmich, "Quantum state transfer between matter and light," Science **306**, 663–666 (2004).
3. W. B. Gao, P. Fallahi, E. Togan, J. Miguel-Sanchez, and A. Imamoglu, "Observation of entanglement between a quantum dot spin and a single photon," Nature **491**, 426–430 (2012).
4. K. De Greve, L. Yu, P. L. McMahon, J. S. Pelc, C. M. Natarajan, N. Y. Kim, E. Abe, S. Maier, C. Schneider, M. Kamp, S. Höfling, R. H. Hadfield, A. Forchel, M. M. Fejer, and Y. Yamamoto, "Quantum-dot spin-photon entanglement via frequency downconversion to telecom wavelength," Nature **491**, 421–425 (2012).
5. E. Togan, Y. Chu, A. S. Trifonov, L. Jiang, J. Maze, L. Childress, M. V. G. Dutt, A. S. Sørensen, P. R. Hemmer, A. S. Zibrov, and M. D. Lukin, "Quantum entanglement between an optical photon and a solid-state spin qubit," Nature **466**, 730–734 (2010).
6. W. F. Koehl, B. B. Buckley, F. J. Heremans, G. Calusine, and D. D. Awschalom, "Room temperature coherent control of defect spin qubits in silicon carbide," Nature **479**, 84–87 (2011).
7. S. M. Girvin, "Circuit QED: superconducting qubits coupled to microwave photons," in *Quantum Machines: Measurement and Control of Engineered Quantum Systems (Les Houches Summer School, Session XCVI)*, M. Devoret, B. Huard, R. Schoelkopf, and L. F. Cugliandolo, eds. (Oxford University, 2014), pp. 113–255.
8. T. Zhong and P. Goldner, "Emerging rare-earth doped material platforms for quantum nanophotonics," Nanophotonics **8**, 2003–2015 (2019).
9. G. Wendin, "Quantum information processing with superconducting circuits: a review," Rep. Prog. Phys. **80**, 106001 (2017).
10. N. Ofek, A. Petrenko, R. Heeres, P. Reinhold, Z. Leghtas, B. Vlastakis, Y. Liu, L. Frunzio, S. M. Girvin, L. Jiang, M. Mirrahimi, M. H. Devoret, and R. J. Schoelkopf, "Extending the lifetime of a quantum bit with error correction in superconducting circuits," Nature **536**, 441–445 (2016).
11. Y. Ma, Y. Xu, X. Mu, W. Cai, L. Hu, W. Wang, X. Pan, H. Wang, Y. P. Song, C.-L. Zou, and L. Sun, "Error-transparent operations on a logical qubit protected by quantum error correction," Nat. Phys. **16**, 827–831 (2020).
12. F. Arute, K. Arya, R. Babbush, D. Bacon, J. C. Bardin, R. Barends, R. Biswas, S. Boixo, F. G. Brandao, D. A. Buell, B. Burkett, Y. Chen, Z. Chen, B. Chiaro, R. Collins, W. Courtney, A. Dunsworth, E. Farhi, B. Foxen, A. Fowler, C. Gidney, M. Giustina, R. Graff, K. Guerin, S. Habegger, M. P. Harrigan, M. J. Hartmann, A. Ho, M. Hoffmann, T. Huang, T. S. Humble, S. V. Isakov, E. Jeffrey, Z. Jiang, D. Kafri, K. Kechedzhi, J. Kelly, P. V. Klimov, S. Knysh, A. Korotkov, F. Kostritsa, D. Landhuis, M. Lindmark, E. Lucero, D. Lyakh, S. Mandrà, J. R. McClean, M. McEwen, A. Megrant, X. Mi, K. Michielsen, M. Mohseni, J. Mutus, O. Naaman, M. Neeley, C. Neill, M. Y. Niu, E. Ostby, A. Petukhov, J. C. Platt, C. Quintana, E. G. Rieffel, P. Roushan, N. C. Rubin, D. Sank, K. J. Satzinger, V. Smelyanskiy, K. J. Sung, M. D. Trevithick, A. Vainsencher, B. Villalonga, T. White, Z. J. Yao, P. Yeh, A. Zalcman, H. Neven, and J. M. Martinis, "Quantum supremacy using a programmable superconducting processor," Nature **574**, 505–510 (2019).
13. "IBM's roadmap for scaling quantum technology," https://www.ibm.com/blogs/research/2020/09/ibm-quantum-roadmap/.
14. H. Takesue, S. D. Dyer, M. J. Stevens, V. Verma, R. P. Mirin, and S. W. Nam, "Quantum teleportation over 100 km of fiber using highly efficient superconducting nanowire single-photon detectors," Optica **2**, 832–835 (2015).
15. J. Yin, Y. Cao, Y.-H. Li, S.-K. Liao, L. Zhang, J.-G. Ren, W.-Q. Cai, W.-Y. Liu, B. Li, H. Dai, G.-B. Li, Q.-M. Lu, Y.-H. Gong, Y. Xu, S.-L. Li, F.-Z. Li, Y.-Y. Yin, Z.-Q. Jiang, M. Li, J.-J. Jia, G. Ren, D. He, and Y.-L. Zhou, "Satellite-based entanglement distribution over 1200 kilometers," Science **356**, 1140–1144 (2017).
16. M. H. Devoret and R. J. Schoelkopf, "Superconducting circuits for quantum information: an outlook," Science **339**, 1169–1174 (2013).
17. Y. Wang, M. Um, J. Zhang, S. An, M. Lyu, J.-N. Zhang, L. M. Duan, D. Yum, and K. Kim, "Single-qubit quantum memory exceeding ten-minute coherence time," Nat. Photonics **11**, 646–650 (2017).
18. T. Astner, J. Gugler, A. Angerer, S. Wald, S. Putz, N. J. Mauser, M. Trupke, H. Sumiya, S. Onoda, J. Isoya, J. Schmiedmayer, P. Mohn, and J. Majer, "Solid-state electron spin lifetime limited by phononic vacuum modes," Nat. Mater. **17**, 313–317 (2018).
19. M. Zhong, M. P. Hedges, R. L. Ahlefeldt, J. G. Bartholomew, S. E. Beavan, S. M. Wittig, J. J. Longdell, and M. J. Sellars, "Optically addressable nuclear spins in a solid with a six-hour coherence time," Nature **517**, 177–180 (2015).
20. Z.-L. Xiang, S. Ashhab, J. You, and F. Nori, "Hybrid quantum circuits: superconducting circuits interacting with other quantum systems," Rev. Mod. Phys. **85**, 623–653 (2013).
21. G. Kurizki, P. Bertet, Y. Kubo, K. Mølmer, D. Petrosyan, P. Rabl, and J. Schmiedmayer, "Quantum technologies with hybrid systems," Proc. Natl. Acad. Sci. USA **112**, 3866–3873 (2015).
22. A. A. Houck, D. I. Schuster, J. M. Gambetta, J. A. Schreier, B. R. Johnson, J. M. Chow, L. Frunzio, J. Majer, M. H. Devoret, S. M. Girvin, and R. J. Schoelkopf, "Generating single microwave photons in a circuit," Nature **449**, 328–331 (2007).
23. Z. H. Peng, S. E. de Graaf, J. S. Tsai, and O. V. Astafiev, "Tuneable on-demand single-photon source in the microwave range," Nat. Commun. **7**, 12588 (2016).
24. K. K. Likharev and V. K. Semenov, "RSFQ logic/memory family: a new Josephson-junction technology for sub-terahertz-clock-frequency digital systems," IEEE Trans. Appl. Supercond. **1**, 3–28 (1991).
25. D. S. Holmes, A. L. Ripple, and M. A. Manheimer, "Energy-efficient superconducting computing-power budgets and requirements," IEEE Trans. Appl. Supercond. **23**, 1701610 (2013).
26. A. Divochiy, F. Marsili, D. Bitauld, A. Gaggero, R. Leoni, F. Mattioli, A. Korneev, V. Seleznev, N. Kaurova, O. Minaeva, G. Gol'tsman, K. G. Lagoudakis, M. Benkhaoul, F. Lévy, and A. Fiore, "Superconducting nanowire photon-number-resolving detector at telecommunication wavelengths," Nat. Photonics **2**, 302–306 (2008).
27. N. J. Lambert, A. Rueda, F. Sedlmeir, and H. G. Schwefel, "Coherent conversion between microwave and optical photons—an overview of physical implementations," Adv. Quantum Technol. **3**, 1900077 (2020).
28. N. Lauk, N. Sinclair, S. Barzanjeh, J. P. Covey, M. Saffman, M. Spiropulu, and C. Simon, "Perspectives on quantum transduction," Quantum Sci. Technol. **5**, 020501 (2020).
29. A. H. Safavi-Naeini, D. V. Thourhout, R. Baets, and R. V. Laer, "Controlling phonons and photons at the wavelength scale: integrated photonics meets integrated phononics: publisher's note," Optica **6**, 410 (2019).
30. Y. Chu and S. Gröblacher, "A perspective on hybrid quantum opto- and electromechanical systems," Appl. Phys. Lett. **117**, 150503 (2020).
31. A. A. Clerk, K. W. Lehnert, P. Bertet, J. R. Petta, and Y. Nakamura, "Hybrid quantum systems with circuit quantum electrodynamics," Nat. Phys. **16**, 257–267 (2020).
32. R. Filip, "Quantum interface to a noisy system through a single kind of arbitrary Gaussian coupling with limited interaction strength," Phys. Rev. A **80**, 022304 (2009).
33. M. Zhang, C.-L. Zou, and L. Jiang, "Quantum transduction with adaptive control," Phys. Rev. Lett. **120**, 020502 (2018).
34. H.-K. Lau and A. A. Clerk, "High-fidelity bosonic quantum state transfer using imperfect transducers and interference," npj Quantum Inf. **5**, 31 (2019).
35. C. Zhong, Z. Wang, C. Zou, M. Zhang, X. Han, W. Fu, M. Xu, S. Shankar, M. H. Devoret, H. X. Tang, and L. Jiang, "Proposal for heralded generation and detection of entangled microwave-optical-photon pairs," Phys. Rev. Lett. **124**, 010511 (2020).
36. D. F. Walls and G. J. Milburn, *Quantum Optics*, 2nd ed. (Springer, 2008).
37. A. A. Clerk, M. H. Devoret, S. M. Girvin, F. Marquardt, and R. J. Schoelkopf, "Introduction to quantum noise, measurement, and amplification," Rev. Mod. Phys. **82**, 1155–1208 (2010).
38. R. W. Andrews, R. W. Peterson, T. P. Purdy, K. Cicak, R. W. Simmonds, C. A. Regal, and K. W. Lehnert, "Bidirectional and efficient conversion between microwave and optical light," Nat. Phys. **10**, 321–326 (2014).
39. M. Xu, X. Han, C.-L. Zou, W. Fu, Y. Xu, C. Zhong, L. Jiang, and H. X. Tang, "Radiative cooling of a superconducting resonator," Phys. Rev. Lett. **124**, 033602 (2020).
40. Z. Wang, M. Xu, X. Han, W. Fu, S. Puri, S. Girvin, H. X. Tang, S. Shankar, and M. Devoret, "Quantum microwave radiometry with a superconducting qubit," Phys. Rev. Lett. **126**, 180501 (2021).
41. B. Abdo, F. Schackert, M. Hatridge, C. Rigetti, and M. Devoret, "Josephson amplifier for qubit readout," Appl. Phys. Lett. **99**, 162506 (2011).
42. B. Abdo, K. Sliwa, F. Schackert, N. Bergeal, M. Hatridge, L. Frunzio, A. D. Stone, and M. Devoret, "Full coherent frequency conversion

between two propagating microwave modes," Phys. Rev. Lett. **110**, 173902 (2013).
43. B. Abdo, A. Kamal, and M. Devoret, "Nondegenerate three-wave mixing with the Josephson ring modulator," Phys. Rev. B **87**, 014508 (2013).
44. B. Abdo, K. Sliwa, S. Shankar, M. Hatridge, L. Frunzio, R. Schoelkopf, and M. Devoret, "Josephson directional amplifier for quantum measurement of superconducting circuits," Phys. Rev. Lett. **112**, 167701 (2014).
45. N. Bergeal, F. Schackert, M. Metcalfe, R. Vijay, V. E. Manucharyan, L. Frunzio, D. E. Prober, R. J. Schoelkopf, S. M. Girvin, and M. H. Devoret, "Phase-preserving amplification near the quantum limit with a Josephson ring modulator," Nature **465**, 64–68 (2010).
46. R. Andrews, A. Reed, K. Cicak, J. Teufel, and K. Lehnert, "Quantum-enabled temporal and spectral mode conversion of microwave signals," Nat. Commun. **6**, 10021 (2015).
47. A. P. Higginbotham, P. S. Burns, M. D. Urmey, R. W. Peterson, N. S. Kampel, B. M. Brubaker, G. Smith, K. W. Lehnert, and C. A. Regal, "Harnessing electro-optic correlations in an efficient mechanical converter," Nat. Phys. **14**, 1038–1042 (2018).
48. G. Arnold, M. Wulf, S. Barzanjeh, E. Redchenko, A. Rueda, W. Hease, F. Hassani, and J. Fink, "Converting microwave and telecom photons with a silicon photonic nanomechanical interface," Nat. Commun. **11**, 4460 (2020).
49. A. Vainsencher, K. J. Satzinger, G. A. Peairs, and A. N. Cleland, "Bi-directional conversion between microwave and optical frequencies in a piezoelectric optomechanical device," Appl. Phys. Lett. **109**, 033107 (2016).
50. W. Jiang, C. J. Sarabalis, Y. D. Dahmani, R. N. Patel, F. M. Mayor, T. P. McKenna, R. Van Laer, and A. H. Safavi-Naeini, "Efficient bidirectional piezo-optomechanical transduction between microwave and optical frequency," Nat. Commun. **11**, 1166 (2020).
51. M. Forsch, R. Stockill, A. Wallucks, I. Marinkovic, C. Gärtner, R. A. Norte, F. van Otten, A. Fiore, K. Srinivasan, and S. Gröblacher, "Microwave-to-optics conversion using a mechanical oscillator in its quantum groundstate," Nat. Phys. **16**, 69–74 (2020).
52. X. Han, W. Fu, C. Zhong, C.-L. Zou, Y. Xu, A. A. Sayem, M. Xu, S. Wang, R. Cheng, L. Jiang, and H. X. Tang, "Cavity piezo-mechanics for superconducting-nanophotonic quantum interface," Nat. Commun. **11**, 3237 (2020).
53. M. Mirhosseini, A. Sipahigil, M. Kalaee, and O. Painter, "Superconducting qubit to optical photon transduction," Nature **588**, 599–603 (2020).
54. P. Kumar, "Quantum frequency conversion," Opt. Lett. **15**, 1476–1478 (1990).
55. R. Salem, M. A. Foster, A. C. Turner, D. F. Geraghty, M. Lipson, and A. L. Gaeta, "Signal regeneration using low-power four-wave mixing on silicon chip," Nat. Photonics **2**, 35–38 (2008).
56. M. T. Rakher, L. Ma, O. Slattery, X. Tang, and K. Srinivasan, "Quantum transduction of telecommunications-band single photons from a quantum dot by frequency upconversion," Nat. Photonics **4**, 786–791 (2010).
57. R. Ikuta, Y. Kusaka, T. Kitano, H. Kato, T. Yamamoto, M. Koashi, and N. Imoto, "Wide-band quantum interface for visible-to-telecommunication wavelength conversion," Nat. Commun. **2**, 537 (2011).
58. J. T. Hill, A. H. Safavi-Naeini, J. Chan, and O. Painter, "Coherent optical wavelength conversion via cavity optomechanics," Nat. Commun. **3**, 1196 (2012).
59. X. Guo, C.-L. Zou, H. Jung, and H. X. Tang, "On-chip strong coupling and efficient frequency conversion between telecom and visible optical modes," Phys. Rev. Lett. **117**, 123902 (2016).
60. J. S. Pelc, L. Yu, K. De Greve, P. L. McMahon, C. M. Natarajan, V. Esfandyarpour, S. Maier, C. Schneider, M. Kamp, S. Höfling, R. H. Hadfield, A. Forchel, Y. Yamamoto, and M. M. Fejer, "Downconversion quantum interface for a single quantum dot spin and 1550-nm single-photon channel," Opt. Express **20**, 27510–27519 (2012).
61. M. M. Wolf, D. Pérez-Garca, and G. Giedke, "Quantum capacities of bosonic channels," Phys. Rev. Lett. **98**, 130501 (2007).
62. C. Wang, C. Langrock, A. Marandi, M. Jankowski, M. Zhang, B. Desiatov, M. M. Fejer, and M. Lončar, "Ultrahigh-efficiency wavelength conversion in nanophotonic periodically poled lithium niobate waveguides," Optica **5**, 1438–1441 (2018).
63. J. Lu, J. B. Surya, X. Liu, A. W. Bruch, Z. Gong, Y. Xu, and H. X. Tang, "Periodically poled thin-film lithium niobate microring resonators with a second-harmonic generation efficiency of 250,000%/w," Optica **6**, 1455–1460 (2019).
64. J. Lu, M. Li, C.-L. Zou, A. Al Sayem, and H. X. Tang, "Toward 1% single-photon anharmonicity with periodically poled lithium niobate microring resonators," Optica **7**, 1654–1659 (2020).
65. A. W. Bruch, X. Liu, X. Guo, J. B. Surya, Z. Gong, L. Zhang, J. Wang, J. Yan, and H. X. Tang, "17 000%/w second-harmonic conversion efficiency in single-crystalline aluminum nitride microresonators," Appl. Phys. Lett. **113**, 131102 (2018).
66. M. Aspelmeyer, T. J. Kippenberg, and F. Marquardt, "Cavity optomechanics," Rev. Mod. Phys. **86**, 1391–1452 (2014).
67. W. Bowen and G. J. Milburn, *Quantum Optomechanics* (CRC Press, 2015).
68. C. A. Regal and K. W. Lehnert, "From cavity electromechanics to cavity optomechanics," J. Phys. Conf. Ser. **264**, 012025 (2011).
69. L. Midolo, A. Schliesser, and A. Fiore, "Nano-opto-electro-mechanical systems," Nat. Nanotechnol. **13**, 11 (2018).
70. J. D. Thompson, B. M. Zwickl, A. M. Jayich, F. Marquardt, S. M. Girvin, and J. G. E. Harris, "Strong dispersive coupling of a high-finesse cavity to a micromechanical membrane," Nature **452**, 72–75 (2008).
71. S. Gröblacher, K. Hammerer, M. R. Vanner, and M. Aspelmeyer, "Observation of strong coupling between a micromechanical resonator and an optical cavity field," Nature **460**, 724–727 (2009).
72. J. D. Teufel, D. Li, M. S. Allman, K. Cicak, A. J. Sirois, J. D. Whittaker, and R. W. Simmonds, "Circuit cavity electromechanics in the strong-coupling regime," Nature **471**, 204–208 (2011).
73. M. Yuan, V. Singh, Y. M. Blanter, and G. A. Steele, "Large cooperativity and microkelvin cooling with a three-dimensional optomechanical cavity," Nat. Commun. **6**, 8491 (2015).
74. M. Yuan, M. A. Cohen, and G. A. Steele, "Silicon nitride membrane resonators at millikelvin temperatures with quality factors exceeding 10^8," Appl. Phys. Lett. **107**, 263501 (2015).
75. Y. Tsaturyan, A. Barg, E. S. Polzik, and A. Schliesser, "Ultracoherent nanomechanical resonators via soft clamping and dissipation dilution," Nat. Nanotechnol. **12**, 776–783 (2017).
76. D. J. Wilson, C. A. Regal, S. B. Papp, and H. J. Kimble, "Cavity optomechanics with stoichiometric sin films," Phys. Rev. Lett. **103**, 207204 (2009).
77. J. D. Teufel, T. Donner, D. Li, J. W. Harlow, M. S. Allman, K. Cicak, A. J. Sirois, J. D. Whittaker, K. W. Lehnert, and R. W. Simmonds, "Sideband cooling of micromechanical motion to the quantum ground state," Nature **475**, 359–363 (2011).
78. R. Peterson, T. Purdy, N. Kampel, R. Andrews, P.-L. Yu, K. Lehnert, and C. Regal, "Laser cooling of a micromechanical membrane to the quantum backaction limit," Phys. Rev. Lett. **116**, 063601 (2016).
79. M. A. Castellanos-Beltran, K. D. Irwin, G. C. Hilton, L. R. Vale, and K. W. Lehnert, "Amplification and squeezing of quantum noise with a tunable Josephson metamaterial," Nat. Phys. **4**, 929–931 (2008).
80. C. Macklin, K. O'Brien, D. Hover, M. E. Schwartz, V. Bolkhovsky, X. Zhang, W. D. Oliver, and I. Siddiqi, "A near-quantum-limited Josephson traveling-wave parametric amplifier," Science **350**, 307–310 (2015).
81. B. H. Eom, P. K. Day, H. G. LeDuc, and J. Zmuidzinas, "A wideband, low-noise superconducting amplifier with high dynamic range," Nat. Phys. **8**, 623–627 (2012).
82. V. V. Sivak, S. Shankar, G. Liu, J. Aumentado, and M. H. Devoret, "Josephson array-mode parametric amplifier," Phys. Rev. Appl. **13**, 024014 (2020).
83. C. M. Caves, "Quantum limits on noise in linear amplifiers," Phys. Rev. D **26**, 1817–1839 (1982).
84. A. D. O'Connell, M. Hofheinz, M. Ansmann, R. C. Bialczak, M. Lenander, E. Lucero, M. Neeley, D. Sank, H. Wang, M. Weides, J. Wenner, J. M. Martinis, and A. N. Cleland, "Quantum ground state and single-phonon control of a mechanical resonator," Nature **464**, 697–703 (2010).
85. S. M. Meenehan, J. D. Cohen, G. S. MacCabe, F. Marsili, M. D. Shaw, and O. Painter, "Pulsed excitation dynamics of an optomechanical crystal resonator near its quantum ground state of motion," Phys. Rev. X **5**, 041002 (2015).
86. S. Hong, R. Riedinger, I. Marinković, A. Wallucks, S. G. Hofer, R. A. Norte, M. Aspelmeyer, and S. Gröblacher, "Hanbury Brown and Twiss interferometry of single phonons from an optomechanical resonator," Science **358**, 203–206 (2017).

87. R. Riedinger, A. Wallucks, I. Marinkovic, C. Löschnauer, M. Aspelmeyer, S. Hong, and S. Gröblacher, "Remote quantum entanglement between two micromechanical oscillators," Nature **556**, 473–477 (2018).
88. H. Ramp, B. Hauer, K. Balram, T. Clark, K. Srinivasan, and J. Davis, "Elimination of thermomechanical noise in piezoelectric optomechanical crystals," Phys. Rev. Lett. **123**, 093603 (2019).
89. F. Rouxinol, Y. Hao, F. Brito, A. Caldeira, E. Irish, and M. LaHaye, "Measurements of nanoresonator-qubit interactions in a hybrid quantum electromechanical system," Nanotechnology **27**, 364003 (2016).
90. X. Han, C. Xiong, K. Y. Fong, X. Zhang, and H. X. Tang, "Triply resonant cavity electro-optomechanics at x-band," New J. Phys. **16**, 063060 (2014).
91. X. Han, C.-L. Zou, and H. X. Tang, "Multimode strong coupling in superconducting cavity piezoelectromechanics," Phys. Rev. Lett. **117**, 123603 (2016).
92. Y. Chu, P. Kharel, W. H. Renninger, L. D. Burkhart, L. Frunzio, P. T. Rakich, and R. J. Schoelkopf, "Quantum acoustics with superconducting qubits," Science **358**, 199–202 (2017).
93. K. J. Satzinger, Y. P. Zhong, H.-S. Chang, G. A. Peairs, A. Bienfait, M.-H. Chou, A. Y. Cleland, C. R. Conner, E. Dumur, J. Grebel, I. Gutierrez, B. H. November, R. G. Povey, S. J. Whiteley, D. D. Awschalom, D. I. Schuster, and A. N. Cleland, "Quantum control of surface acoustic-wave phonons," Nature **563**, 661–665 (2018).
94. Y. Chu, P. Kharel, T. Yoon, L. Frunzio, P. T. Rakich, and R. J. Schoelkopf, "Creation and control of multi-phonon Fock states in a bulk acoustic-wave resonator," Nature **563**, 666–670 (2018).
95. P. Arrangoiz-Arriola, E. A. Wollack, Z. Wang, M. Pechal, W. Jiang, T. P. McKenna, J. D. Witmer, R. V. Laer, and A. H. Safavi-Naeini, "Resolving the energy levels of a nanomechanical oscillator," Nature **571**, 537–540 (2019).
96. A. Bienfait, K. J. Satzinger, Y. P. Zhong, H.-S. Chang, M.-H. Chou, C. R. Conner, É. Dumur, J. Grebel, G. A. Peairs, R. G. Povey, and A. N. Cleland, "Phonon-mediated quantum state transfer and remote qubit entanglement," Science **364**, 368–371 (2019).
97. M. Eichenfield, J. Chan, R. M. Camacho, K. J. Vahala, and O. Painter, "Optomechanical crystals," Nature **462**, 78–82 (2009).
98. J. Chan, T. P. M. Alegre, A. H. Safavi-Naeini, J. T. Hill, A. Krause, S. Gröblacher, M. Aspelmeyer, and O. Painter, "Laser cooling of a nanomechanical oscillator into its quantum ground state," Nature **478**, 89–92 (2011).
99. J. Chan, A. H. Safavi-Naeini, J. T. Hill, S. Meenehan, and O. Painter, "Optimized optomechanical crystal cavity with acoustic radiation shield," Appl. Phys. Lett. **101**, 081115 (2012).
100. K. C. Balram, M. Davanço, J. Y. Lim, J. D. Song, and K. Srinivasan, "Moving boundary and photoelastic coupling in GaAs optomechanical resonators," Optica **1**, 414–420 (2014).
101. K. C. Balram, M. I. Davanço, J. D. Song, and K. Srinivasan, "Coherent coupling between radiofrequency, optical and acoustic waves in piezo-optomechanical circuits," Nat. Photonics **10**, 346–352 (2016).
102. W. Jiang, R. N. Patel, F. M. Mayor, T. P. McKenna, P. Arrangoiz-Arriola, C. J. Sarabalis, J. D. Witmer, R. V. Laer, and A. H. Safavi-Naeini, "Lithium niobate piezo-optomechanical crystals," Optica **6**, 845–853 (2019).
103. X. Han, K. Y. Fong, and H. X. Tang, "A 10-GHz film-thickness-mode cavity optomechanical resonator," Appl. Phys. Lett. **106**, 161108 (2015).
104. M. Shen, J. Xie, C.-L. Zou, Y. Xu, W. Fu, and H. X. Tang, "High frequency lithium niobate film-thickness-mode optomechanical resonator," Appl. Phys. Lett. **117**, 131104 (2020).
105. M. Tomes and T. Carmon, "Photonic micro-electromechanical systems vibrating at X-band (11-GHz) rates," Phys. Rev. Lett. **102**, 113601 (2009).
106. I. S. Grudinin, A. B. Matsko, and L. Maleki, "Brillouin lasing with a CaF_2 whispering gallery mode resonator," Phys. Rev. Lett. **102**, 043902 (2009).
107. P. Kharel, Y. Chu, E. A. Kittlaus, N. T. Otterstrom, S. Gertler, and P. T. Rakich, "Multimode strong coupling in cavity optomechanics," arXiv:1812.06202v2 (2018).
108. P. Kharel, G. I. Harris, E. A. Kittlaus, W. H. Renninger, N. T. Otterstrom, J. G. E. Harris, and P. T. Rakich, "High-frequency cavity optomechanics using bulk acoustic phonons," Sci. Adv. **5**, eaav0582 (2019).
109. H. Tian, J. Liu, B. Dong, J. C. Skehan, M. Zervas, T. J. Kippenberg, and S. A. Bhave, "Hybrid integrated photonics using bulk acoustic resonators," Nat. Commun. **11**, 3073 (2020).
110. J. Bochmann, A. Vainsencher, D. D. Awschalom, and A. N. Cleland, "Nanomechanical coupling between microwave and optical photons," Nat. Phys. **9**, 712–716 (2013).
111. M. Wu, E. Zeuthen, K. C. Balram, and K. Srinivasan, "Microwave-to-optical transduction using a mechanical supermode for coupling piezoelectric and optomechanical resonators," Phys. Rev. Appl. **13**, 014027 (2020).
112. G. S. MacCabe, H. Ren, J. Luo, J. D. Cohen, H. Zhou, A. Sipahigil, M. Mirhosseini, and O. Painter, "Nano-acoustic resonator with ultralong phonon lifetime," Science **370**, 840–843 (2020).
113. H. Ren, M. H. Matheny, G. S. MacCabe, J. Luo, H. Pfeifer, M. Mirhosseini, and O. Painter, "Two-dimensional optomechanical crystal cavity with high quantum cooperativity," Nat. Commun. **11**, 3373 (2020).
114. T. P. McKenna, J. D. Witmer, R. N. Patel, W. Jiang, R. V. Laer, P. Arrangoiz-Arriola, E. A. Wollack, J. F. Herrmann, and A. H. Safavi-Naeini, "Cryogenic microwave-to-optical conversion using a triply resonant lithium-niobate-on-sapphire transducer," Optica **7**, 1737–1745 (2020).
115. J. Holzgrafe, N. Sinclair, D. Zhu, A. Shams-Ansari, M. Colangelo, Y. Hu, M. Zhang, K. K. Berggren, and M. Lončar, "Cavity electro-optics in thin-film lithium niobate for efficient microwave-to-optical transduction," Optica **7**, 1714–1720 (2020).
116. Y. Xu, A. A. Sayem, L. Fan, C.-L. Zou, S. Wang, R. Cheng, W. Fu, L. Yang, M. Xu, and H. X. Tang, "Bidirectional interconversion of microwave and light with thin-film lithium niobate," Nat. Commun. **12**, 4453 (2021).
117. L. Fan, C.-L. Zou, R. Cheng, X. Guo, X. Han, Z. Gong, S. Wang, and H. X. Tang, "Superconducting cavity electro-optics: a platform for coherent photon conversion between superconducting and photonic circuits," Sci. Adv. **4**, eaar4994 (2018).
118. W. Fu, M. Xu, X. Liu, C.-L. Zou, C. Zhong, X. Han, M. Shen, Y. Xu, R. Cheng, S. Wang, L. Jiang, and H. X. Tang, "Cavity electro-optic circuit for microwave-to-optical conversion in the quantum ground state," Phys. Rev. A **103**, 053504 (2021).
119. M. Tsang, "Cavity quantum electro-optics," Phys. Rev. A **81**, 063837 (2010).
120. M. Tsang, "Cavity quantum electro-optics. II. Input-output relations between traveling optical and microwave fields," Phys. Rev. A **84**, 043845 (2011).
121. C. Javerzac-Galy, K. Plekhanov, N. R. Bernier, L. D. Toth, A. K. Feofanov, and T. J. Kippenberg, "On-chip microwave-to-optical quantum coherent converter based on a superconducting resonator coupled to an electro-optic microresonator," Phys. Rev. A **94**, 053815 (2016).
122. M. Soltani, M. Zhang, C. Ryan, G. J. Ribeill, C. Wang, and M. Loncar, "Efficient quantum microwave-to-optical conversion using electro-optic nanophotonic coupled resonators," Phys. Rev. A **96**, 043808 (2017).
123. A. Rueda, F. Sedlmeir, M. C. Collodo, U. Vogl, B. Stiller, G. Schunk, D. V. Strekalov, C. Marquardt, J. M. Fink, O. Painter, G. Leuchs, and H. G. L. Schwefel, "Efficient microwave to optical photon conversion: an electro-optical realization," Optica **3**, 597–604 (2016).
124. W. Hease, A. Rueda, R. Sahu, M. Wulf, G. Arnold, H. G. L. Schwefel, and J. M. Fink, "Bidirectional electro-optic wavelength conversion in the quantum ground state," PRX Quantum **1**, 020315 (2020).
125. J. D. Witmer, J. A. Valery, P. Arrangoiz-Arriola, C. J. Sarabalis, J. T. Hill, and A. H. Safavi-Naeini, "High-Q photonic resonators and electro-optic coupling using silicon-on-lithium-niobate," Sci. Rep. **7**, 46313 (2017).
126. M. Zhang, C. Wang, R. Cheng, A. Shams-Ansari, and M. Lončar, "Monolithic ultra-high-Q lithium niobate microring resonator," Optica **4**, 1536–1537 (2017).
127. J. Holzgrafe, N. Sinclair, D. Zhu, A. Shams-Ansari, M. Colangelo, Y. Hu, M. Zhang, K. K. Berggren, and M. Loncar, "Toward efficient microwave-optical transduction using cavity electro-optics in thin-film lithium niobate," in *Conference on Lasers and Electro-Optics (CLEO)* (2020), pp. 1–2.
128. X. Zhang, N. Zhu, C.-L. Zou, and H. X. Tang, "Optomagnonic whispering gallery microresonators," Phys. Rev. Lett. **117**, 123605 (2016).

129. X. Zhang, N. Zhu, C.-L. Zou, and H. X. Tang, "Erratum: Optomagnonic whispering gallery microresonators [phys. rev. lett. 117, 123605 (2016)]," Phys. Rev. Lett. **121**, 199901 (2018).
130. R. Hisatomi, A. Osada, Y. Tabuchi, T. Ishikawa, A. Noguchi, R. Yamazaki, K. Usami, and Y. Nakamura, "Bidirectional conversion between microwave and light via ferromagnetic magnons," Phys. Rev. B **93**, 174427 (2016).
131. N. Zhu, X. Zhang, X. Han, C.-L. Zou, C. Zhong, C.-H. Wang, L. Jiang, and H. X. Tang, "Waveguide cavity optomagnonics for microwave-to-optics conversion," Optica **7**, 1291–1297 (2020).
132. N. Zhu, X. Zhang, X. Han, C.-L. Zou, and H. X. Tang, "Inverse faraday effect in an optomagnonic waveguide," arXiv:1909.12295v2 (2021).
133. X. Zhang, C.-L. Zou, L. Jiang, and H. X. Tang, "Strongly coupled magnons and cavity microwave photons," Phys. Rev. Lett. **113**, 156401 (2014).
134. Y. Tabuchi, S. Ishino, A. Noguchi, T. Ishikawa, R. Yamazaki, K. Usami, and Y. Nakamura, "Coherent coupling between a ferromagnetic magnon and a superconducting qubit," Science **349**, 405–408 (2015).
135. D. Lachance-Quirion, Y. Tabuchi, S. Ishino, A. Noguchi, T. Ishikawa, R. Yamazaki, and Y. Nakamura, "Resolving quanta of collective spin excitations in a millimeter-sized ferromagnet," Sci. Adv. **3**, e1603150 (2017).
136. J. Bourhill, N. Kostylev, M. Goryachev, D. L. Creedon, and M. E. Tobar, "Ultrahigh cooperativity interactions between magnons and resonant photons in a YIG sphere," Phys. Rev. B **93**, 144420 (2016).
137. J. A. Haigh, A. Nunnenkamp, A. J. Ramsay, and A. J. Ferguson, "Triple-resonant Brillouin light scattering in magneto-optical cavities," Phys. Rev. Lett. **117**, 133602 (2016).
138. C. Kittel, "Excitation of spin waves in a ferromagnet by a uniform RF field," Phys. Rev. **112**, 2139 (1958).
139. D. D. Awschalom, R. Hanson, J. Wrachtrup, and B. B. Zhou, "Quantum technologies with optically interfaced solid-state spins," Nat. Photonics **12**, 516–527 (2018).
140. X. Fernandez-Gonzalvo, Y.-H. Chen, C. Yin, S. Rogge, and J. J. Longdell, "Coherent frequency up-conversion of microwaves to the optical telecommunications band in an Er:YSO crystal," Phys. Rev. A **92**, 062313 (2015).
141. X. Fernandez-Gonzalvo, S. P. Horvath, Y.-H. Chen, and J. J. Longdell, "Cavity-enhanced Raman heterodyne spectroscopy in Er^{3+}:Y_2SiO_5 for microwave to optical signal conversion," Phys. Rev. A **100**, 033807 (2019).
142. J. G. Bartholomew, J. Rochman, T. Xie, J. M. Kindem, A. Ruskuc, I. Craiciu, M. Lei, and A. Faraon, "On-chip coherent microwave-to-optical transduction mediated by ytterbium in YVO_4," Nat. Commun. **11**, 3266 (2020).
143. K. Adwaith, A. Karigowda, C. Manwatkar, F. Bretenaker, and A. Narayanan, "Coherent microwave-to-optical conversion by three-wave mixing in a room temperature atomic system," Opt. Lett. **44**, 33–36 (2019).
144. T. Vogt, C. Gross, J. Han, S. B. Pal, M. Lam, M. Kiffner, and W. Li, "Efficient microwave-to-optical conversion using Rydberg atoms," Phys. Rev. A **99**, 023832 (2019).
145. Z.-B. Feng, H.-L. Wang, and R.-Y. Yan, "Quantum state transfer between an optomechanical cavity and a diamond nuclear spin ensemble," Quantum Inf. Process. **15**, 3151–3167 (2016).
146. I. Lekavicius, D. A. Golter, T. Oo, and H. Wang, "Transfer of phase information between optical and microwave fields via an electron spin," arXiv:1705.00093 (2017).
147. C. O'Brien, N. Lauk, S. Blum, G. Morigi, and M. Fleischhauer, "Interfacing superconducting qubits and telecom photons via a rare-earth-doped crystal," Phys. Rev. Lett. **113**, 063603 (2014).
148. L. A. Williamson, Y.-H. Chen, and J. J. Longdell, "Magneto-optic modulator with unit quantum efficiency," Phys. Rev. Lett. **113**, 203601 (2014).
149. J. R. Everts, M. C. Berrington, R. L. Ahlefeldt, and J. J. Longdell, "Microwave to optical photon conversion via fully concentrated rare-earth ion crystals," Phys. Rev. A **99**, 063830 (2019).
150. A. S. Zibrov, A. B. Matsko, and M. O. Scully, "Four-wave mixing of optical and microwave fields," Phys. Rev. Lett. **89**, 103601 (2002).
151. J. Verdú, H. Zoubi, C. Koller, J. Majer, H. Ritsch, and J. Schmiedmayer, "Strong magnetic coupling of an ultracold gas to a superconducting waveguide cavity," Phys. Rev. Lett. **103**, 043603 (2009).
152. M. Kiffner, A. Feizpour, K. T. Kaczmarek, D. Jaksch, and J. Nunn, "Two-way interconversion of millimeter-wave and optical fields in Rydberg gases," New J. Phys. **18**, 093030 (2016).
153. B. T. Gard, K. Jacobs, R. McDermott, and M. Saffman, "Microwave-to-optical frequency conversion using a cesium atom coupled to a superconducting resonator," Phys. Rev. A **96**, 013833 (2017).
154. J. Han, T. Vogt, C. Gross, D. Jaksch, M. Kiffner, and W. Li, "Coherent microwave-to-optical conversion via six-wave mixing in Rydberg atoms," Phys. Rev. Lett. **120**, 093201 (2018).
155. Y. Wang, J. Li, S. Zhang, K. Su, Y. Zhou, K. Liao, S. Du, H. Yan, and S.-L. Zhu, "Efficient quantum memory for single-photon polarization qubits," Nat. Photonics **13**, 346–351 (2019).
156. R. Yan, G. Khalsa, S. Vishwanath, Y. Han, J. Wright, S. Rouvimov, D. S. Katzer, N. Nepal, B. P. Downey, D. A. Muller, H. G. Xing, D. J. Meyer, and D. Jena, "GaN/NbN epitaxial semiconductor/superconductor heterostructures," Nature **555**, 183–189 (2018).
157. R. Cheng, J. Wright, H. G. Xing, D. Jena, and H. X. Tang, "Epitaxial niobium nitride superconducting nanowire single-photon detectors," Appl. Phys. Lett. **117**, 132601 (2020).
158. O. Černotík, S. Mahmoodian, and K. Hammerer, "Spatially adiabatic frequency conversion in optoelectromechanical arrays," Phys. Rev. Lett. **121**, 110506 (2018).
159. P. Rakich and F. Marquardt, "Quantum theory of continuum optomechanics," New J. Phys. **20**, 045005 (2018).
160. A. Rueda, W. Hease, S. Barzanjeh, and J. M. Fink, "Electro-optic entanglement source for microwave to telecom quantum state transfer," npj Quantum Inf. **5**, 108 (2019).
161. C. Zhong, X. Han, H. X. Tang, and L. Jiang, "Entanglement of microwave-optical modes in a strongly coupled electro-optomechanical system," Phys. Rev. A **101**, 032345 (2020).